We are IntechOpen,
the world's leading publisher of
Open Access books
Built by scientists, for scientists

4,800
Open access books available

122,000
International authors and editors

135M
Downloads

Our authors are among the

154
Countries delivered to

TOP 1%
most cited scientists

12.2%
Contributors from top 500 universities

CLARIVATE ANALYTICS
BOOK CITATION INDEX
INDEXED

WEB OF SCIENCE™

Selection of our books indexed in the Book Citation Index
in Web of Science™ Core Collection (BKCI)

Interested in publishing with us?
Contact book.department@intechopen.com

Numbers displayed above are based on latest data collected.
For more information visit www.intechopen.com

The Sintering Behaviour of Fe-Mn-C Powder System, Correlation between Thermodynamics and Sintering Process, Manganese Distribution and Microstructure Composition, Effect of Alloying Mode

Eduard Hryha[1] and Eva Dudrova[2]
[1]Chalmers University of Technology, Gothenburg
[2]Institute of Materials Research, Slovak Academy of Sciences, Košice
[1]Sweden
[2]Slovak Republic

1. Introduction

Among steel-making techniques Powder Metallurgy (PM) concept utilizes unique production cycle, consisting of powder compaction and sintering steps that give high productivity with low energy consumption and high material utilization. Due to the presence of residual porosity, mechanical properties of PM components are inferior in comparison with structural components produced by other technologies. Improvement of mechanical properties at the same level of porosity can be achieved primarily by adding variety of alloying elements. Therefore modern PM technology for production of high-performance PM parts for highly stressed steel components for automotive industry, for example, rely on techniques of utilization of different alloying elements additionally to adjustment of technological process depending on alloying system used. When talking about high-strength low-alloyed structural steels, the most common alloying elements, additionally to carbon, added in order to increase mechanical performance, are chromium, manganese, silicon and some other strong carbide and carbonitride-forming elements (V, Nb, Ti etc.). In comparison with classical steelmaking practice, alloying of PM steels is much more complicated as additionally to influence of alloying elements type and content on microstructure, mechanical properties, hardenability etc., number of additional aspects influencing powder production and further component processing has to be considered. Traditionally, PM high-strength steels are alloyed with Cu, Ni, and Mo. This results in a considerable difference in price of material between conventional and PM steels, used for the same high-load application, as the price of currently employed PM alloying elements like Mo and Ni is dozens of times higher in comparison with that of Cr or Mn. This situation creates a strong economical stimulation to introduce cheaper and more efficient alloying elements to improve the competitiveness of PM structural parts.

So, why the potential of most common for conventional metallurgy alloying elements as Cr, Mn and Si is not utilized in PM? First and basic question that arise is how to introduce these

elements in PM – as admixed elemental powder (or master-alloy) or by prealloying of the base steel powder. Chromium prealloyed steels are already successfully introduced on the PM market. However due to the peculiar properties of manganese (oxygen affinity, high vapour pressure, ferrite strengthening etc.) attempts to develop Mn sintered steels are still ongoing. Issue of appropriate alloying mode, that is the starting point of manganese introduction in PM, is the basic question that has to be answered at the beginning and is the basic topic of this chapter.

The easiest way to introduce manganese is by admixing of ferromanganese powder that is cheap and widely available on the market in different grades. This approach was firstly proposes around 30 years ago and have been scrutinized thoroughly from different perspectives (Šalak, 1980; Cias et al., 1999; Šalak et al., 2001; Dudrova et al., 2004; Danninger et al., 2005; Cias&Wronski, 2008, Hryha, 2007). The first thing that has to be considered when dealing with admixed with manganese systems is high affinity of manganese to oxygen, implying possibility of considerable oxidation during component processing due to high activity of manganese in admixed elemental powder. However, the possibility of sintering of admixed with manganese powders was assumed due to so-called ''self-cleaning'' effect, discovered by Šalak (Šalak, 1980). This effect utilizes unique property of manganese to sublimate at relatively low temperature and created during heating stage manganese vapour protects specimen from further oxidation. Another advantage of admixed manganese systems is manganese homogenization in Fe–Mn powder compacts involving Mn-gaseous phase during the heating stage. Second assumption deals with the alloying by different master-alloys that firstly allowed a successful introduction of high oxygen affinity elements in PM industrial production (Zapf et al., 1975; Schlieper & Thummler, 1979; Hoffmann & Dalal, 1979). First developed master-alloys containing manganese–chromium–molybdenum (MCM) and manganese–vanadium–molybdenum (MVM) had a wide range of mechanical properties depending on alloying content, sintered density and processing conditions. Nevertheless, these master-alloys faced with many problems during application (oxides formation during manufacturing process, high hardness of the particles that lead to intensive wear of compacting tools etc.) and fully disappeared from manufacturing and research areas. Recent development of Fe–Cr–Mn–Mo–C master-alloys was much more successful and show promising properties for their future industrial utilization (Beiss, 2006; Sainz et al., 2006).

High affinity of manganese for oxygen and Mn loss by sublimation can be minimized by lowering the manganese activity that can be done by Mn introduction in pre-alloyed state. However powder alloying by manganese faces some difficulties starting from powder production, handling and following compaction and sintering steps. This is connected with manganese selective oxidation on the powder surface during atomization and further annealing depending on processing conditions during powder production (Hryha et al., 2009-b; Hryha et al., 2010-a). A further negative impact of manganese utilization in pre-alloyed state is the expected lower compressibility of such pre-alloyed powders due to ferrite solid solution strengthening by manganese.

This chapter is focused on the influence of alloying mode, utilizing premix systems with different ferromanganese grades and high-purity electrolytic manganese as well as fully prealloying of water atomized powder. While respecting all the benefits and problems with sintered steels alloyed with manganese some basic directions have been chosen — theoretical evaluations of required sintering atmosphere composition for preventing of manganese

alloyed steels from oxidation during every stage of sintering, analyzes of sintering cycle coupled with simultaneous atmosphere monitoring and further analysis of sintered specimens using number of advanced spectroscopy and thermoanalytic techniques. Various phenomena, connected with manganese evaporation and reduction/oxidation behaviour of manganese alloyed sintered steels were theoretically evaluated and tested experimentally applying interrupted sintering experiments, when specimens where sampled at different stages of the sintering cycle for extensive study by HR SEM+EDX, XPS, TG+MS etc. Thermodynamic calculations enabled to determine a required sintering atmosphere composition (maximal permitted partial pressures of active gases $CO/CO_2/H_2O$) for preventing of Mn alloyed steels prepared by different alloying mode from oxidation during every stage of sintering. The results were verified by continual monitoring of $CO/CO_2/H_2O$ profiles in sintering atmosphere and further analysis of sintered specimens.

2. Thermodynamic evaluation of Mn-containing PM steels

2.1 Manganese sublimation

The first effect that has to be considered when talking about manganese containing steels is manganese sublimation. High amount of manganese vapour at elevated temperatures determines number of interrelated processes such as manganese distribution through the pore system, manganese loss and its oxidation through reaction with oxygen and water vapour in the local atmosphere. Intensive manganese sublimation starts already at around 700°C when its partial pressure reaches about 10^{-3} Pa, see Fig.1. Further temperature increasing leads to exponential increasing of manganese partial pressure, that at conventional sintering temperature of 1120°C reaches about 20 Pa.
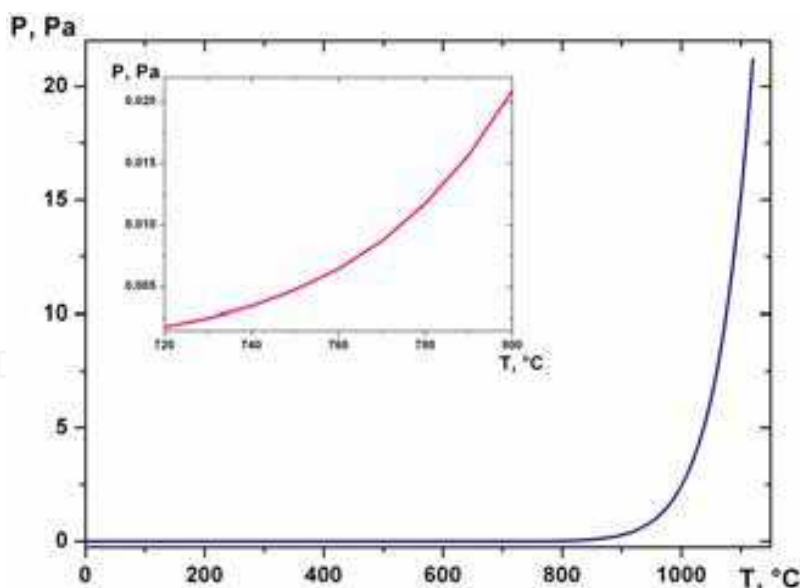

Fig. 1. Equilibrium partial pressure of Mn_{gas} with temperature, *HSC Chemistry 6.1*

2.2 Oxidation of manganese vapour

It is important to emphasize that at such low temperatures partial pressures of active gases inside pore system has to be incredibly low in order to prevent Mn vapour from oxidation, as it is evident from Ellingham-Richardsson diagram, see Fig.2. Dew-point below -95°C at 700°C is required in typically used in industry $10\%H_2/90\%N_2$ sintering atmosphere to

prevent Mn vapour from oxidation that is impossible even in laboratory conditions in powder compact. Phase stability diagram in Mn-O-H and Mn-O-C systems, see Fig.3, indicate that even at typically used in industry sintering temperature of 1120°C in nitrogen/hydrogen atmosphere in presence of admixed graphite oxygen partial pressure below 10^{-21} bar is required to as minimum prevent manganese from oxidation. Diagrams in Fig.3 also indicate that at applied during sintering conditions MnO is the most stable oxide and during all further thermodynamic calculation was considered as only one manganese oxide presented in the system.
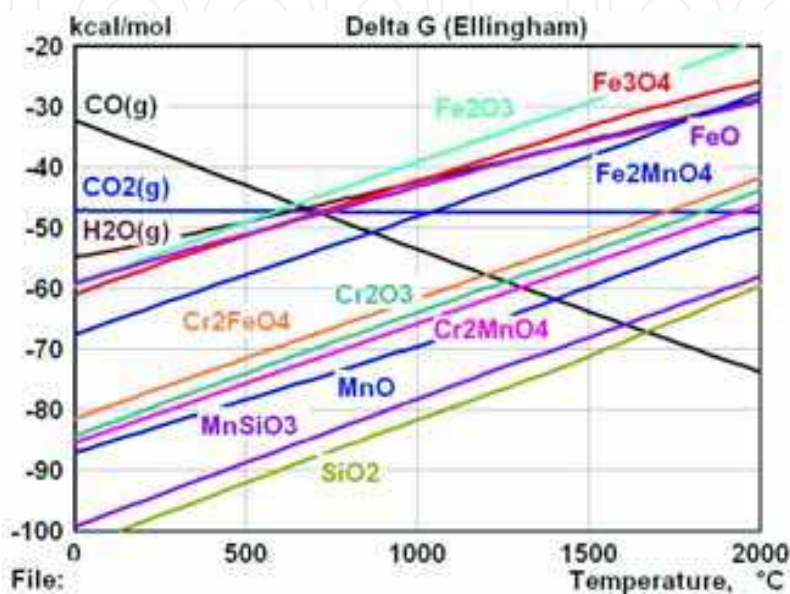
Fig. 2. Ellingham-Richardson diagram indicating stability of oxides
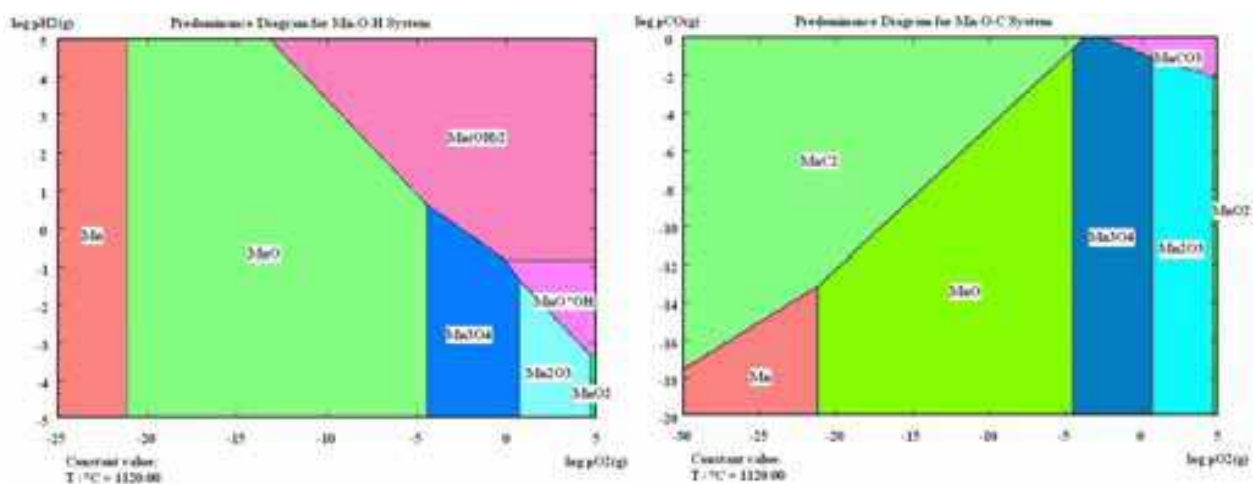

Fig. 3. Mn-O-H (left) and Mn-O-C (right) phase stability diagrams, *HSC Chemistry 6.1*

Produced at higher temperature manganese vapour reacts with the oxygen in the processing atmosphere according to the following reaction:

$$2Mn_{(gas)}+O_2=2MnO \qquad (1)$$

Depending on the oxygen partial pressure in the surrounding manganese source specimen 'microclimate', the reaction between the $Mn_{(gas)}$ and oxygen occurs on different distance. If

in the pore system, surrounding manganese source, oxygen partial pressure is higher than equilibrium partial pressure at defined temperature, that is the case during heating stage, manganese vapour will be oxidised close to the manganese carrier particle and manganese oxide will condense on the surface of the surrounding base powder particles. If local microclimate is pure enough, oxidation of manganese vapour take place at larger distances from manganese source, that further purify 'microclimate' conditions and allows transport of manganese through the gas phase in the range of this microclimate, its condensation and further dissolution into base iron powder particles. This is the mechanism of 'self-cleaning' effect described by Šalak (Šalak, 1980), however it is important to note that it leads to desirable 'microclimate' purification preferentially in dry atmospheres and high temperatures, when oxygen partial pressure is slightly higher than equilibrium one. When considering strong oxidising conditions, especially at low temperatures when manganese starts to sublimate and have still rather low partial pressure and oxygen partial pressure at the same time is much higher than equilibrium one, all the available $Mn_{(gas)}$ in the system is oxidised that does not lead to considerable microclimate purification. Extensive manganese oxidation at higher oxygen partial pressure was experimentally observed by *(Šalak, 1980)* that include the formation of a greenish MnO film on the surface of compacts. Another fact that is important to underline is that at the intermediate temperatures (600-900°C), when manganese actually starts to sublimate, local 'microclimate' conditions inside the powder compact are much worse than in the processing atmosphere applied because considerable amount of oxygen is released by the reduction of the surface iron oxide from the base powder. Oxygen, produced by the reduction of surface iron oxide, can be released in different forms depending on sintering technique applied (vacuum or atmosphere sintering, utilizing inert or hydrogen containing atmosphere). When considering vacuum sintering dissociation of iron oxide is one of the dominant mechanism (when carbon is not present or inactive at low temperatures) and oxygen is released. However, most typically manganese PM steels are sintered in hydrogen-containing atmospheres, where due to reduction of iron oxide by hydrogen water vapour is produced. Importance of the reaction of manganese vapour with water vapour was emphasized by (Cias et al., 1999). This reaction results in the formation of H_2 in the microclimate through the reaction:

$$Mn_{(gas)}+H_2O_{(vapour)} =MnO+H_2 \qquad (2)$$
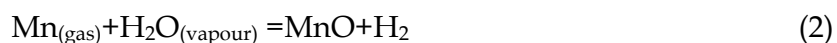
and also leads to further atmosphere purification, but, at the same time – considerable manganese vapour oxidation. Nevertheless, there is one more mechanism that leads to more considerable manganese vapour oxidation, especially at inter-mediate temperatures. As it was shown by (Danninger et al., 2002) for a number of iron and alloyed PM steels, and by (Hryha et al., 2010-a) for a manganese prealloyed PM steels, above ~600°C, depending on alloying element type and content, carbothermal reduction of iron surface oxide layer starts, leading to production of carbon monoxide. This carbon monoxide is also oxidising agent for manganese vapour at low temperatures at observed high partial pressures, registered by (Hryha, 2007), according to reaction:

$$Mn_{(gas)}+CO=MnO+C \qquad (3)$$
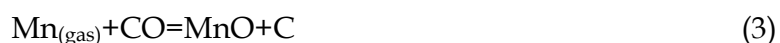
According to this reaction from *HSC Chemistry 6.1* database as minimum to prevent manganese vapour from oxidation, carbon monoxide partial pressure has to be below ~$6.3*10^{-7}$ (bar) at 700°C. However, during atmosphere monitoring of sintering process for

manganese containing PM steels (Hryha, 2007) CO-content in the sintering atmosphere was in the range from 10^{-4} to 10^{-3} (bar), clearly indicating oxidation of Mn-vapour. It is important to emphasize that situation inside the pores is even more oxidizing and if sintering is performed with bad processing atmosphere control (low purity/flow), formation of carbon dioxide at inter-mediate temperatures is possible creating even more harmful oxidising conditions. This is the reason why 'self-cleaning' effect does not actually work at inter-mediate temperatures.
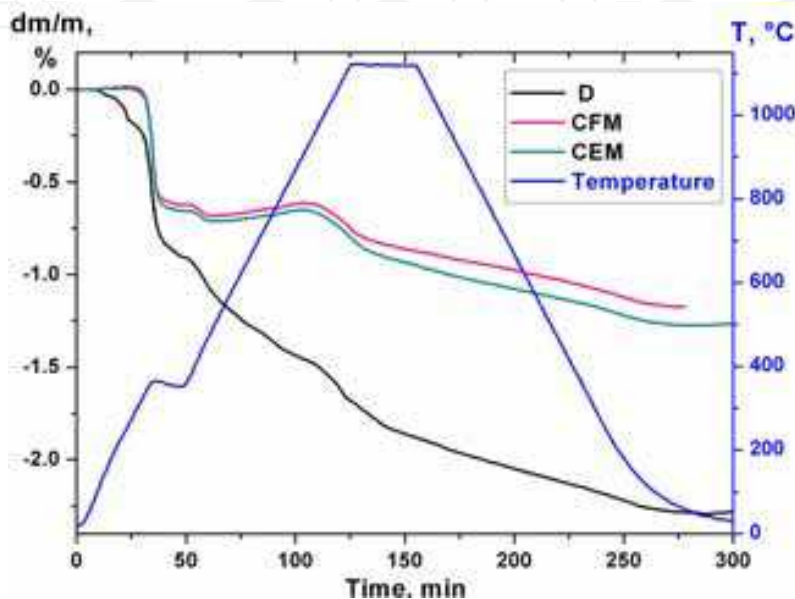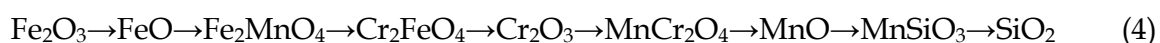

Fig. 4. Thermogravimetry graphs for admixed with electrolytic manganese (**CEM**) and ferromanganese (**CFM)** materials in comparison with fully prealloyed material (**D)** of the same composition Fe-0.8Mn-0.5C

Intensive manganese oxidation at medium temperatures is evident even on thermal analysis (Hryha, 2007), especially when comparing with the material based on fully prealloyed powder. The mass-change curves are very similar for both admixed specimens, see Fig.4, but huge difference in comparison with the pre-alloyed material is evident. First high mass loss is observed during heating up to 350°C, including the de-waxing holding, and is connected preferably with lubricant removal and desorption of the physically bonded water. During further heating up to 500°C higher mass loss was detected for prealloyed material – reduction of the iron oxide layer on the powder surface by the hydrogen. The much lower mass-loss in the case of admixed specimens points at their potential oxidation. Temperature increasing up to ~900°C results in increase of the samples mass for admixed specimens – oxidation of manganese carrier particles/manganese vapour as high mass-loss was observed in the case of prealloyed material. After ~920°C high mass-losses were observed for all three materials connected with the carbothermal reduction of the more stable surface oxides and internal oxides for all three materials.

As it was mentioned above, the product of this reaction is fine dispersed MnO that is condensed on the free powder surfaces and hampers the development of interparticle connections. To avoid the formation of oxide networks, Cias (Cias et al., 2003) proposed a method employing a semiclosed container to create an active "microclimate" around and within the Fe-Mn-C compacts. Another alternative is sintering in a hydrogen atmosphere with low enough dew point dictated by the Ellingham–Richardson diagram. As it was

emphasized above, in the hydrogen-rich sintering atmosphere it is important to maintain both high atmosphere purity and adequate gas flow to minimize content of water vapour, formed by surface iron oxide reduction. From the Ellingham-Richardson diagram, Fig.2, it is also evident that temperature increasing leads to improved thermodynamic conditions that allows to prevent manganese vapour from intensive oxidation and application of high sintering temperatures (1200-1250°C) allows successful sintering of admixed manganese steels as even reduction of manganese oxides is possible in hydrogen-containing atmospheres in modern sintering furnaces.

Presented in Fig.2 Ellingham-Richardson diagram also emphasize presence in the system and high stability of mixed oxides of spinel type, that are important to take into consideration as iron/steel powders always contain trace amounts of Cr and Si, and formation at high temperatures and presence of these oxides were experimentally confirmed by (Hryha et al., 2010-a). Especially it is important to emphasize presence of Cr-Mn and Mn-Si oxides that due to the lack of experimental information and absence of thermodynamic data were disregarded during previous studies of oxidation/reduction behaviour of Mn and Cr-Mn PM steels. Based on the presented in Fig.2 diagram and the discussion above, the stability of oxides presented in Cr-Mn alloyed PM materials increases in the line:

$$Fe_2O_3 \rightarrow FeO \rightarrow Fe_2MnO_4 \rightarrow Cr_2FeO_4 \rightarrow Cr_2O_3 \rightarrow MnCr_2O_4 \rightarrow MnO \rightarrow MnSiO_3 \rightarrow SiO_2 \qquad (4)$$

Detailed study of the thermodynamics of reduction of the presented mixed oxides in the case of powders pre-alloyed with Cr and Mn is presented elsewhere (*Hryha et al., 2010*).

2.3 Thermodynamic evaluation of sintering requirements

Process conditions for the successful sintering can be calculated based on simple algorithms for reaction energies calculations (Gaskell, 2003). Mitchell (Mitchell & Cias, 2004) performed such calculations for some chromium and manganese containing PM steels. Algorithm and theoretical evaluation of the required atmosphere composition at every sintering stage for manganese contained PM steels in more details are also presented by (Hryha et al., 2010-b).

Sintering atmosphere composition required was evaluated based on standard free-energy calculations using a thermodynamic software package *Outotech HSC Chemistry 6.1*. Calculations are performed for the oxidation/reduction reactions for the oxide that is in direct contact with atmosphere – condensed manganese vapour located on the base powder particles surface. Carbon during calculations was considered as pure non-dissolved graphite admixed to the base powder. According to these considerations, the activities of the surface oxides and carbon can be taken as unity. As the most stable oxide in the system is MnO, see Figs.2 and 3, thermodynamic requirements, calculated for the reduction of this oxide, will meet the thermodynamic requirements for less stable iron and iron-manganese oxides.

The algorithm of the calculations is based on evaluation of maximum pressures of active gases, which can be tolerated in the system for as minimum avoiding oxidation of manganese, at the sintering temperature. The calculations are based on evaluation of free energy for each reaction at the defined sintering temperature based on $\Delta G_T^0 = \Delta H - T\Delta S$.

Using relationship $\Delta G_T^0 = -RT \ln K_p$ equilibrium constant for each reaction can be calculated and partial pressures of active gases can be easily evaluated. Four basic chemical reactions were taken into consideration:

$$MnO = Mn + 0.5O_2 \qquad (5)$$

$$MnO+C=Mn+CO \tag{6}$$

$$C+CO_2=2CO \tag{7}$$

$$2CO+O_2=2CO_2 \tag{8}$$

$$C+H_2O=CO+H_2 \tag{9}$$

These reactions allow establish equilibrium partial pressures of the most important active gases in the system (oxygen, water vapour, carbon monoxide and carbon dioxide). Based on these calculations it was shown (Hryha et al., 2010-b) that in the case of sintering in nitrogen/10% hydrogen atmosphere at 1120°C for MnO, Mn and C to be in equilibrium with a gaseous atmosphere, this atmosphere must be of composition:

$P(CO)= 1.674*10^{-2}$ bar

$P(CO_2)=5.16*10^{-7}$ bar

$P(O_2)=7.18*10^{-22}$ bar

$P(H_2O)=6.75*10^{-6}$ (bar)

Water partial pressure $P(H_2O)= 6.75*10^{-6}$ bar corresponds to a dew-point near -63°C. This points on the fact that a dew-point lower than -63°C is required for proper sintering of manganese containing steels in the $90\%N_2/10\%H_2$ atmosphere at 1120°C.

Sintering temperature increasing to 1200°C put less strict requirements on the sintering atmosphere purity:

$P(CO)=6.09 *10^{-2}$ bar

$P(CO_2)=3.13*10^{-6}$ bar

$P(O_2)=2.79*10^{-20}$ bar

$P(H_2O)=1.3*10^{-5}$ bar (DP≈- 58°C)

easily achievable in a modern sintering furnaces. It is important to note that for inert atmospheres or atmospheres with hydrogen content other than 10% equilibrium pressure of water vapour has to be re-evaluated.

It is important to state that the pre-alloyed powder do not have such strict requirements to the atmosphere purity due to the much lower manganese activity in the prealloyed state. This means that the activity of manganese in the case of the prealloyed powder can be taken equal to its content according to Henry's law (Gaskell, 2003) that will decrease maximum allowed pressures of active gases for about one-two orders. However, it has to be taken into account that presented calculations are still valid when considering necessity of full reduction of manganese particulate oxides on the surface of prealloyed powder, (Hryha et al., 2010-b).

2.4 Liquid phase formation in the Fe-Mn-C system

Šalak (Šalak 1980-a and Šalak 1980-b) experimentally identified one more specific feature of manganese alloying when using high-carbon ferromanganese that is concerned with

presence of liquid manganese alloy phase that occurs at certain circumstances at sintering
temperatures. Many further detailed observation of fracture surface of Fe-Mn-C PM
materials (Hryha, 2007, Dudrova et al., 2010) confirms presence of a transient liquid phase in
the areas of prior ferromanganese particle surfaces. Such liquid phase formation was not
registered in Fe-Mn-C steel when high-purity electrolytic manages was used as the
manganese source (Hryha, 2007). Detailed thermodynamic analysis of low melting point
alloys by Gomez-Acebo (Gomez-Acebo et al., 2003) in the case of Fe-Mn-C system using the
Thermo-Calc software reveals lowest melting point for the alloy composition Fe-30.3Mn-
4.03C at 1077°C. The thermodynamic calculations of the equilibrium isothermal section for
the ternary Fe-Mn-C alloy system at 1120°C using Thermo-Calc together with SSOL2
thermodynamic database, Fig. 5, displays a rather extended liquid phase region close to the
sintering temperature. Clearly, intensive manganese evaporation during heating together
with iron and carbon diffusion into ferromanganese residue can lead to liquid phase
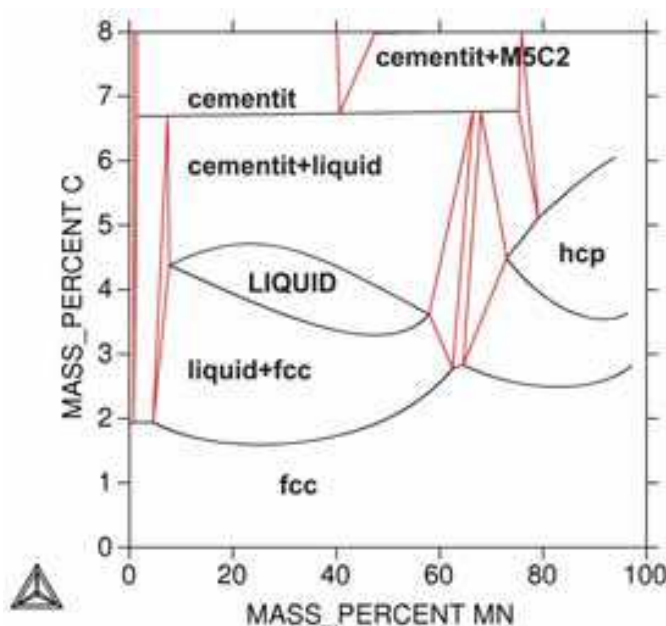formation at around 1120°C for high-carbon and even medium carbon ferromanganese.

Fig. 5. Equilibrium isothermal section for the Fe-Mn-C alloy system at 1120°C (Thermo-Calc,
SSOL2 database)

3. Microstructure development and composition

Tracing of microstructure development during sintering process (heating stage and different
dwelling times) proofs itself to be a powerful tool when studying powder systems (Hryha
2007, Dudrova et al., 2010). It allows to trace reduction of surface iron oxide layer, carbon
and manganese dissolution and so microstructure development, oxides distribution etc. To
be able to follow processes carefully during heating stage, specimens were slowly heated (10
°C·min^{-1}) up to the sintering temperature of 1120/1200°C, and sampled at defined
temperatures, as it is shown in Fig.6, and cooled at the cooling rate of 10 or 50 K·min^{-1} to
room temperature. Due to the lubricant presence, the specimens were additionally held at
~350°C for de-lubrication. First two sampling temperatures were chosen below the α→γ
transition (onset on dilatometry curve) and next one above transition temperature (offset on
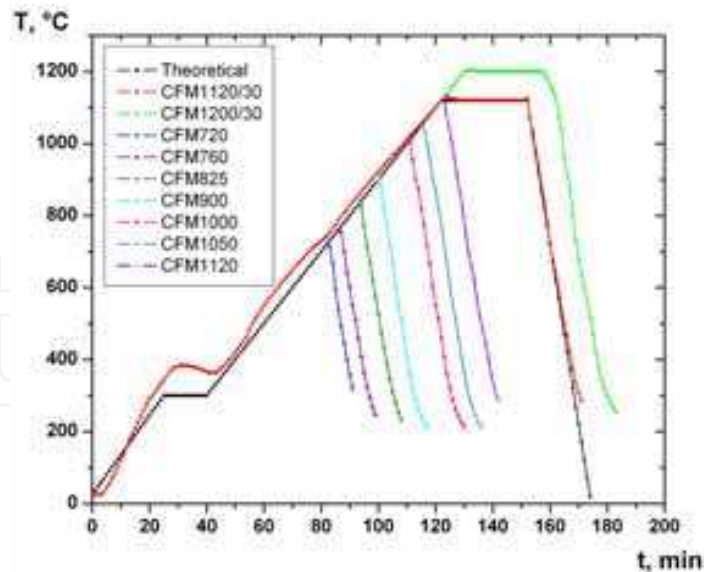dilatometry curve) measured for the studied alloys, (Hryha, 2007).

Fig. 6. Thermo-profile during interrupted sintering trials

Microstructure development processes differs considerably for pre-mixed powder systems, where manganese was added as high-purity electrolytic manganese powder and medium carbon ferromanganese powder, compared with fully prealloyed powder (Hryha, 2007; Hryha et al., 2010-b). As an example, Fig.7 presents microstructure development and composition in the case of admixed with ferromanganese powder system, marked as **CFM**. Heterogeneous ferritic-pearlitic microstructure is characteristic for all sampled at different sintering stages specimens, see Fig. 7. Some coarse pearlite on the grain boundaries near the edges of prior particles extending up to 10 μm was registered after the interrupted sintering at 825°C and its fraction is about 10% at 900°C. Austenitic rims around Mn carrier particles were registered and were shown to have a thickness of up to 1 μm after the 760°C run, ~3 μm after the 825°C run, up to ~4 μm after the 900°C run and about 5 μm for the sampled at 1000°C specimen, indicating rather pronounced Mn dissolution in the iron matrix with increasing temperature. Ferromanganese particles can be observed in material processed up to the sintering temperature. Nevertheless at the beginning of the sinter-holding manganese carriers are shown to occur only as large pores with pronounced "sponge" structure, filled by contaminants. This indicates that manganese is already distributed throughout the surrounding pore system. The fraction of fine pearlite reaches about 20%. The complicated sequence of microstructure constituents around the Mn-residues (austenite that changes to martensite and mixture of upper and lower bainite and pearlite at larger distances from the FeMn particles) was firstly observed at 1120°C and shown to extend up to 10-12 μm from the Mn-carrier particles. After sintering for 30 min at 1120°C, pronounced Mn dissolution in the Fe matrix is evident resulting in the extension of the austenite-martensite-bainite mixture up to 20 μm followed by a more extended pearlite region, while the core of the prior iron particles is still fully ferritic. The pronounced difference between the slow and fast cooled specimens, sintered at 1120°C, is evident in lower portion of pearlite in the slowly cooled one. This is also a result of lower as-sintered carbon content in slowly cooled specimen related to the higher carbon loss due to more oxidising conditions during the slow cooling. The oxidation of the slowly cooled specimen was clearly seen on a non-etched microstructure. The specimens sintered at higher temperature (1200°C) show more homogeneous austenite-martensite mixture in the areas adjoining to residue. The bainitic

areas pass into pearlitic rims around ferromanganese residue. Due to the large size of admixed ferromanganese particles even after sintering rather large pores (up to 20 µm) filled with contaminants were observed. The same microstructure heterogeneity as for the admixed with ferromanganese alloy is characteristic for the admixed with electrolytic manganese alloy for all temperatures. The microstructure development includes the same features as the admixed with the ferromanganese system, however more extended dissolution of manganese during heating stage was registered for admixed with electrolytic manganese system, showing austenitic rims nearly twice as thick around electrolytic manganese in comparison with FeMn, see (Hryha et al., 2010-b).
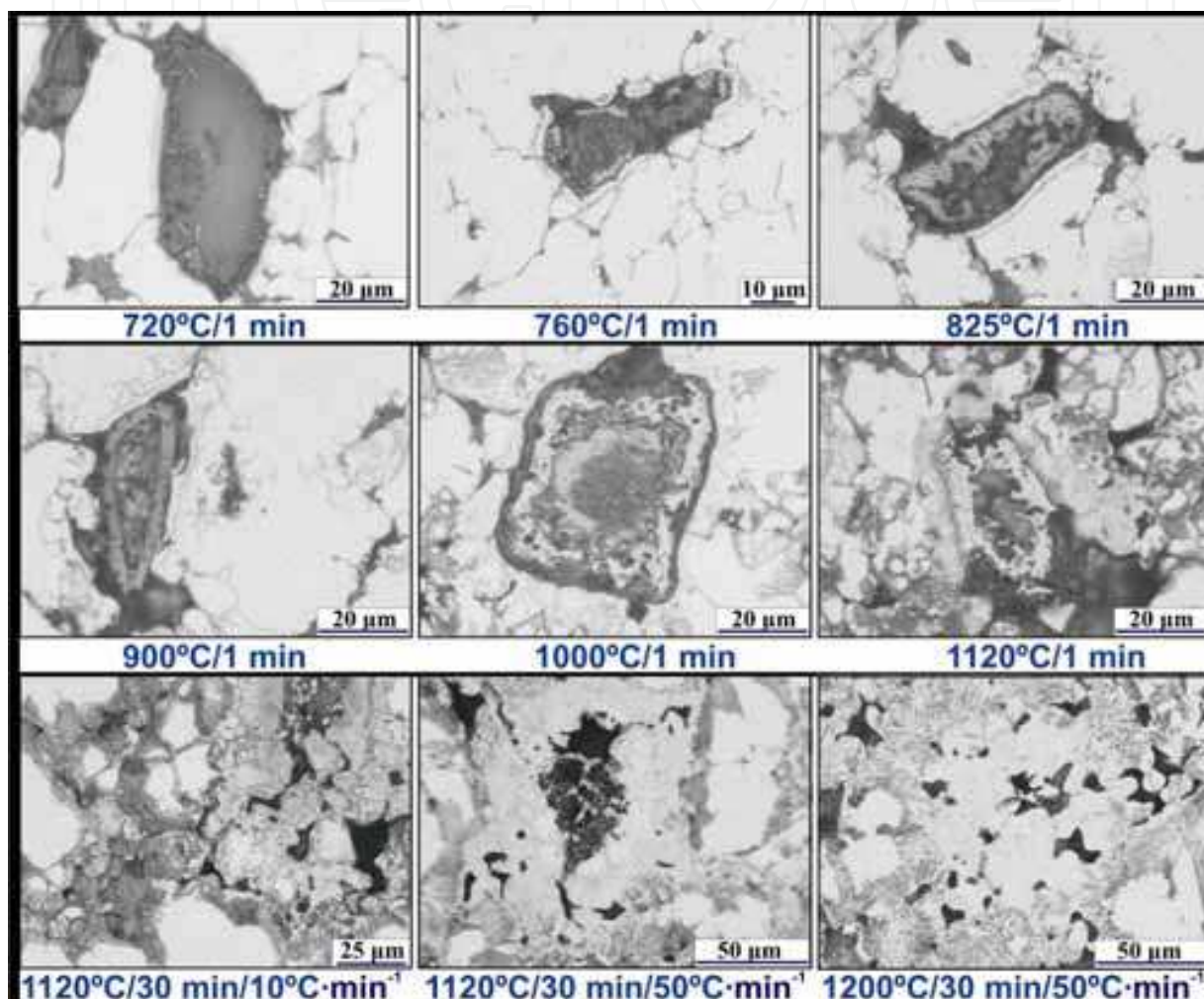
Fig. 7. Microstructure development during sintering of admixed with ferromanganese powder system Fe-0.8Mn-0.5C

The development of the microstructure with increasing temperature and its final state in the case of the pre-alloyed material differs significantly from the admixed systems with the same chemical composition (Fe-0.8Mn-0.5C) and processing conditions (Hryha et al., 2009-a and Hryha et al., 2010-b). Higher purity and presence of some pearlite close to the edges of prior particles was observed even for the first sampled specimen at 740ºC, indicating much faster carbon transport in this system in comparison with the admixed one, see Fig.8. After the 810ºC run, the pearlite extends up to 10 µm; the comparable amount and distribution of the pearlite for admixed systems was observed only after the 900ºC run. After the 900ºC-

processing of the pre-alloyed material, fine pearlite is evenly distributed in the iron matrix and its fraction is ~ 20%; such pronounced carbon distribution was observed for the admixed system only after processing close to the sintering temperature. Further temperature increasing leads to pearlite portion increasing to 30-35% after the 1000°C run and to about 40% after the 1120°C run that are comparable with the results regarding the as-sintered microstructure of admixed alloy. Then, sintering of the pre-alloyed material at 1120°C for 30 min results in evenly distributed ferrite-pearlite mixture where fine pearlite is prevailing and its portion is up to 55-60%. Higher oxidation of the slow-cooled specimen after sintering at 1120°C was registered as well, with a little bit lower portion of pearlite being coarser than in the case of fast cooled specimen, see Fig.8. Sintering at 1200°C gave microstructure comparable to sintered at 1120°C compact. Distinguishing feature of the prealloyed material is more rounded, smaller and pure pores in comparison with the admixed one.
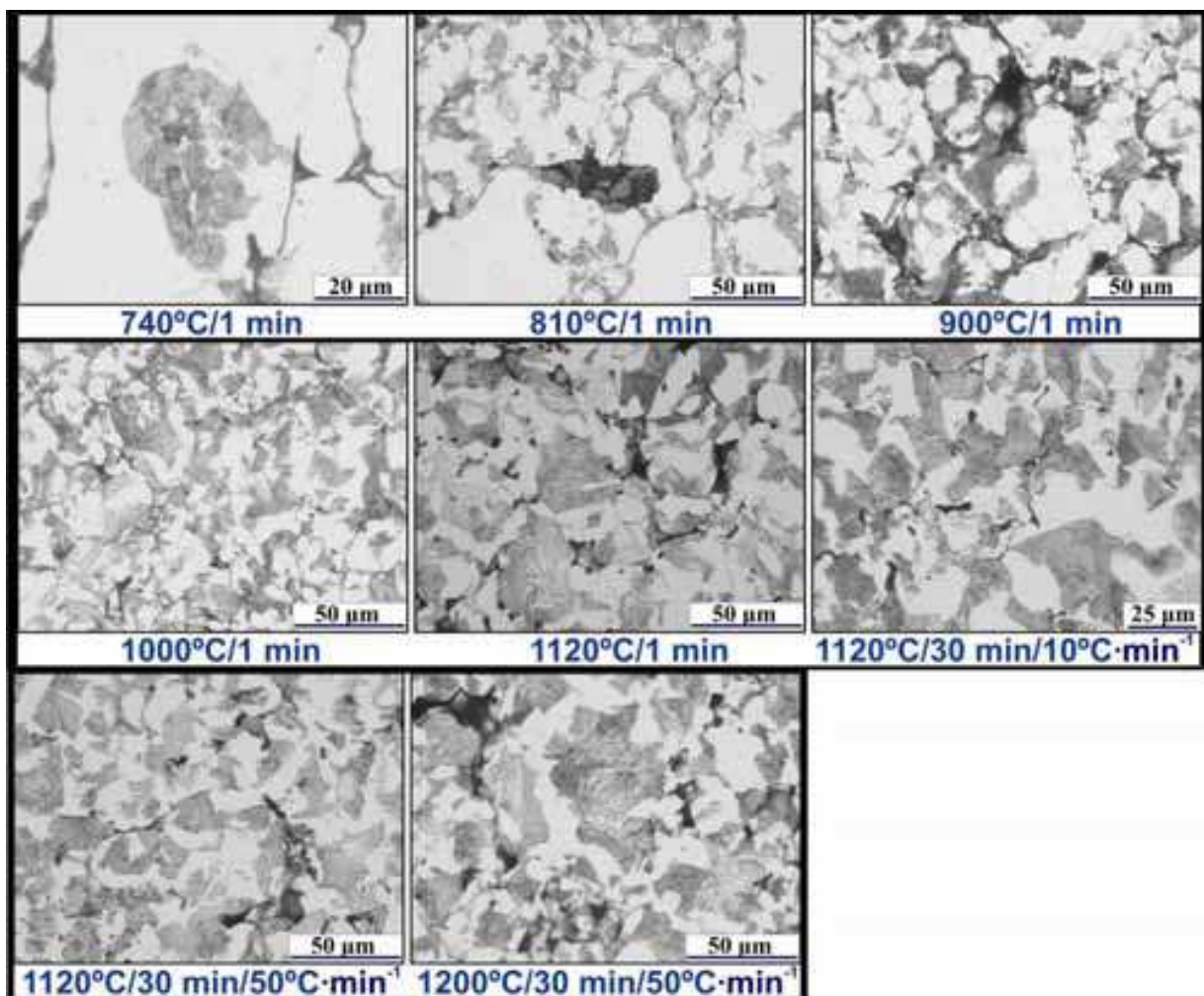

Fig. 8. Microstructure development during sintering of prealloyed powder system Fe-0.8Mn-0.5C

Additionally effect of manganese content on microstructure development was studied on prealloyed powder with higher manganese content of 1.8 wt.% (Hryha et al., 2009-a). The microstructure of this material indicates appearance of some pearlite near the edges of the prior particles even after the 710°C run, see Fig.9. Temperature increasing leads to higher pearlite portion, being about 20% after the 790°C run, and after 900°C run a structure

consists of evenly distributed ferrite-pearlite with pearlite fraction about 35%. After the
1000°C run, an almost fully fine-pearlitic microstructure was obtained. This was not
observed for any of the materials mentioned. The pearlite had a very fine lamellae structure
distinguishable only at high resolution. After reaching of sintering temperature (1120°C), a
bainitic microstructure starts to occur and after sintering for 30 min at this temperature the
bainite fraction is 10-15 wt.%. The microstructure of the specimens sintered at 1200°C
consists of evenly distributed and very fine ferrite-carbide mixture, where the bainitic
microstructure is dominant (<50%). Distinguishing features of this alloy are higher pearlite
fraction at all temperatures as well as its much finer structure than observed for the
prealloyed with 0.8 wt.% Mn material at all temperatures.
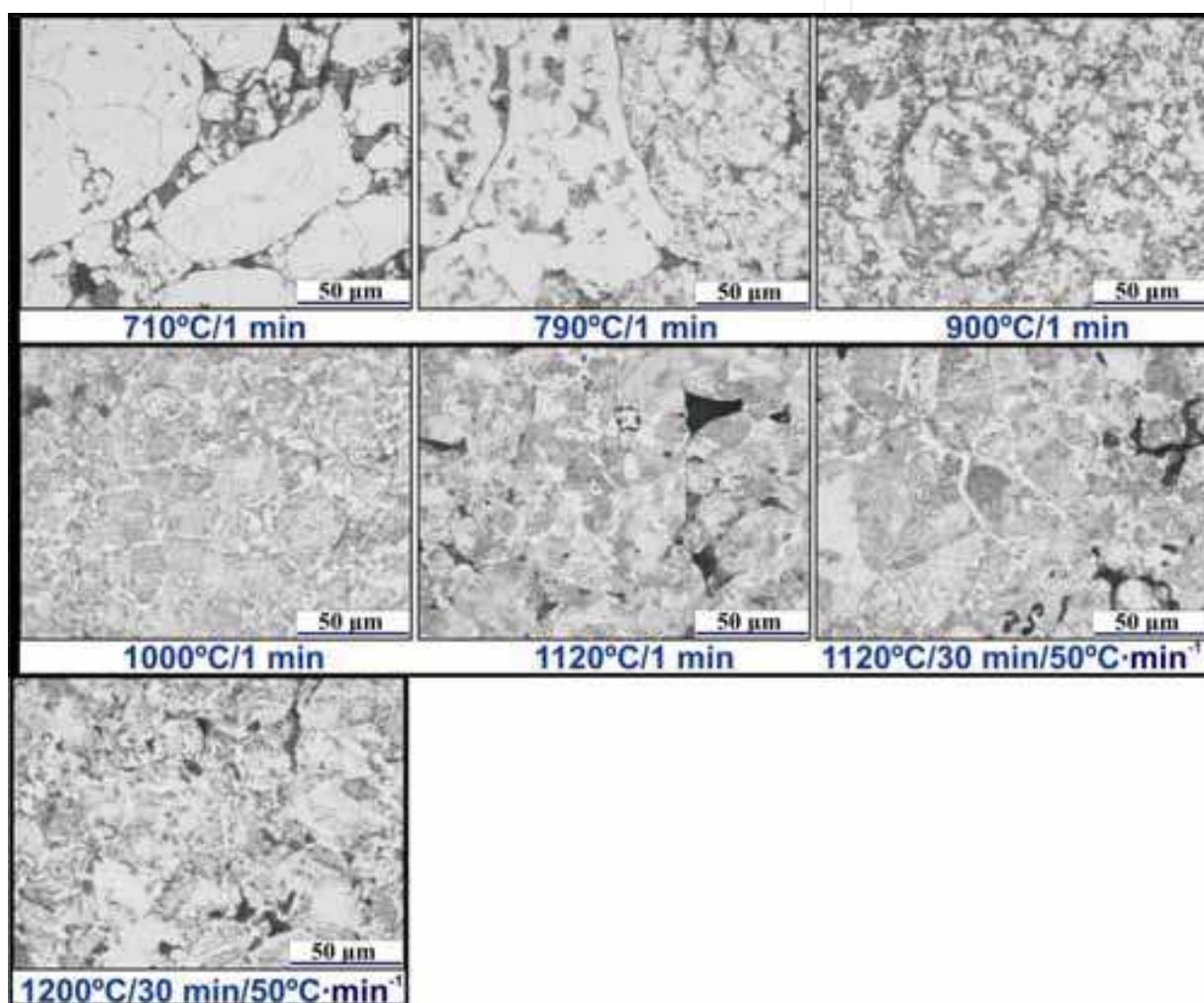
Fig. 9. Microstructure development during sintering of prealloyed powder system Fe-
1.8Mn-0.5C

4. Manganese distribution

When comparing microstructure development between the admixed with the ferromanganese
and electrolytic manganese systems, detected thickness of the Mn-enriched areas was nearly
twice as thick around electrolytic manganese in comparison with the FeMn. Additionally,
when comparing measured values during heating stage (increasing from 2-4 µm at 750°C up to

~8 μm at 1000°C) with the calculated depth of Mn solution in the iron matrix in this range of temperatures based on literature data, (Dudrova et al., 2010), see Table 1, it is clearly evident that detected values are as minimum one order of magnitude larger.

The fact that manganese dissolution depth calculated based on the only diffusion mechanism is clearly underestimated was also confirmed by careful measurements of the manganese concentration profiles using energy and wave dispersive X-ray analyses (EDX and WDX, respectively), (Hryha, 2007). Presented in Fig.10 SEM micrograph of ferromanganese residue in the Fe-0.8Mn-0.5C material, sintered at 1120°C for 30 min in nitrogen/hydrogen atmosphere, with marked line of EDX analysis, show that FeMn residue is a complex contaminations, formed by MnS and complex Fe-Mn-Si-O oxides. Line EDX analysis shows gradient in manganese concentration in the areas around FeMn residue. As line EDX analysis gives only relative information about elements distribution, quantitative analysis of Mn-concentration profile was performed by WDX analysis in the area around FeMn residue, see Fig.11. Mn concentration profiles clearly shows manganese enriched area up to ~30 μm from the iron particle edge (Hryha&Dudrova, 2007; Hryha, 2007).

Composition, %Mn/%C	T/t, °C /min	D_{Mn}, $cm^2 s^{-1}$	Reference*	Mn diffusion depths, μm
Mn in α-Fe, 0/0	770/3	7.0481×10^{-15}	*Nohara&Hirano, 1971*	0.00113
Mn in α-Fe, 20/0	770/3	3.8965×10^{-14}	*Wells&Mehl, 1941*	0.02648
Mn in γ-Fe	1040/3	6.2110×10^{-12}	*Nohara&Hirano, 1971*	0.3344
Mn in γ-Fe, 10/0	1040/3	6.0604×10^{-12}	*Wells&Mehl, 1941*	0.3303
Mn in γ-Fe	1080/3	1.2619×10^{-11}	*Nohara&Hirano, 1971*	0.4766
Mn in γ-Fe, 10/0	1080/3	1.2808×10^{-11}	*Wells&Mehl, 1941*	0.4663
Mn in γ-Fe	1170/3	5.3847×10^{-11}	*Nohara&Hirano, 1971*	0.9845
Mn in γ-Fe, 10/0	1170/3	5.9270×10^{-11}	*Wells&Mehl, 1941*	1.0329
Mn in γ-Fe	1220/3	1.1179×10^{-10}	*Nohara&Hirano, 1971*	1.4185
Mn in γ-Fe, 10/0	1220/3	1.6060×10^{-10}	*Wells&Mehl, 1941*	1.7002
Mn in γ-Fe	1220/30	1.1179×10^{-10}	*Nohara&Hirano, 1971*	4.4858
Mn in γ-Fe, 10/0	1220/30	1.6060×10^{-10}	*Wells&Mehl, 1941*	5.3766

Table 1. Literature Mn diffusion coefficients D_{Mn} and calculated Mn diffusion depths x in iron lattice for temperature range 770–1220°C ; $x=(D_{Mn} \times t)^{1/2}$

Results show the manganese content in the range 2-4 at.% at the distances of about 20-30 μm from the manganese carrier residue. It has to be emphasized that such a large deviation of measured Mn content from the place to place is caused by two main reasons: size of the initial ferromanganese particle (amount of the capable to diffusion manganese) and geometry of the iron particles cut where analysis is performed. There is a high probability of

existing pore close under analyzed area, meaning contribution from manganese dissolution from the manganese layer beneath (caused by manganese transport in the adjoining to FeMn particle pores by manganese vapor phase). This also describes such a 'wavy' character of measured manganese profiles, see Fig.11. This means that large number of concentration profiles has to be measured to obtain statistically correct values for evaluation of manganese dissolution depth in Fe-Mn PM steels.
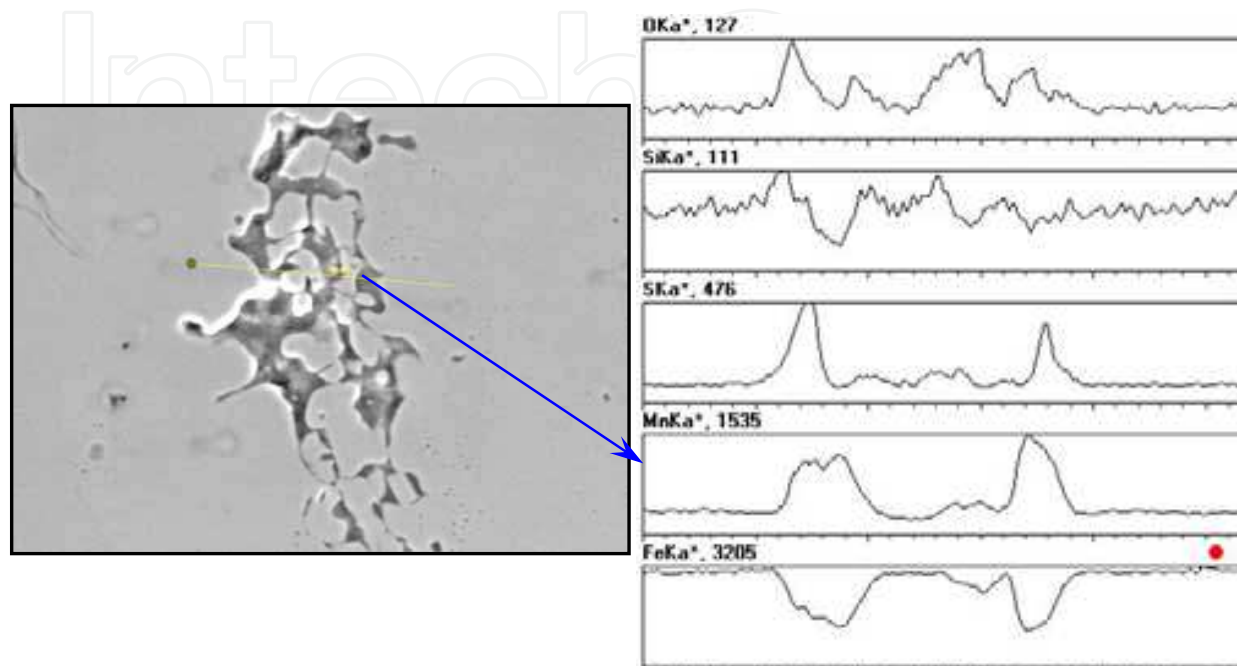

Fig. 10. SEI image of ferromanganese residue for Fe-0.8Mn-0.5C specimen, sintered at 1120°C for 30 min, with marked line of Energy Dispersive X-ray analysis and results of line analysis of O, Si, S, Mn and Fe distribution

Nevertheless, it is no doubt that the observed depth of manganese alloyed areas around manganese carrier particles is much larger than volume diffusion could account for. Even if considering that manganese isoconcentration lines are parallel to the iron particle boundaries, that can point to volume diffusion as the dominant mechanism, its just can be assumed inappropriateness of applying of presented in literature volume diffusion coefficient to the powder Fe-Mn system. However, diffusion profile calculated based on only volume diffusion gives very steep concentration profile (Navara, 1980), contrary to the smooth concentration gradient observed. When discussing manganese dissolution it is important to remember Mn-transport through the gas phase (Mn-vapour). Comparable effect of improved diffusivity of several orders of magnitude in the presence of gas phase was firstly observed by (Hillert&Purdy, 1977), in the case of iron-zinc materials in the atmosphere of zinc. They clearly showed that much higher diffusivity observed is a result of combination of a grain boundary diffusion and chemically induced grain boundary migration (DIGM). Another important conclusion by (Hillert&Purdy, 1977), is that grain boundary diffusion is 2-4 orders of magnitude enhanced by the movement of the grain boundary, that together leads to considerable enhancement of the dissolution depth. The hypothesis about application of alloying mechanism with the presence of the gas phase, as in the case of iron-zinc system, for iron-manganese system, was firstly proposed by Navara (Navara, 1980*)* and further developed by Šalak (Šalak, 1989).
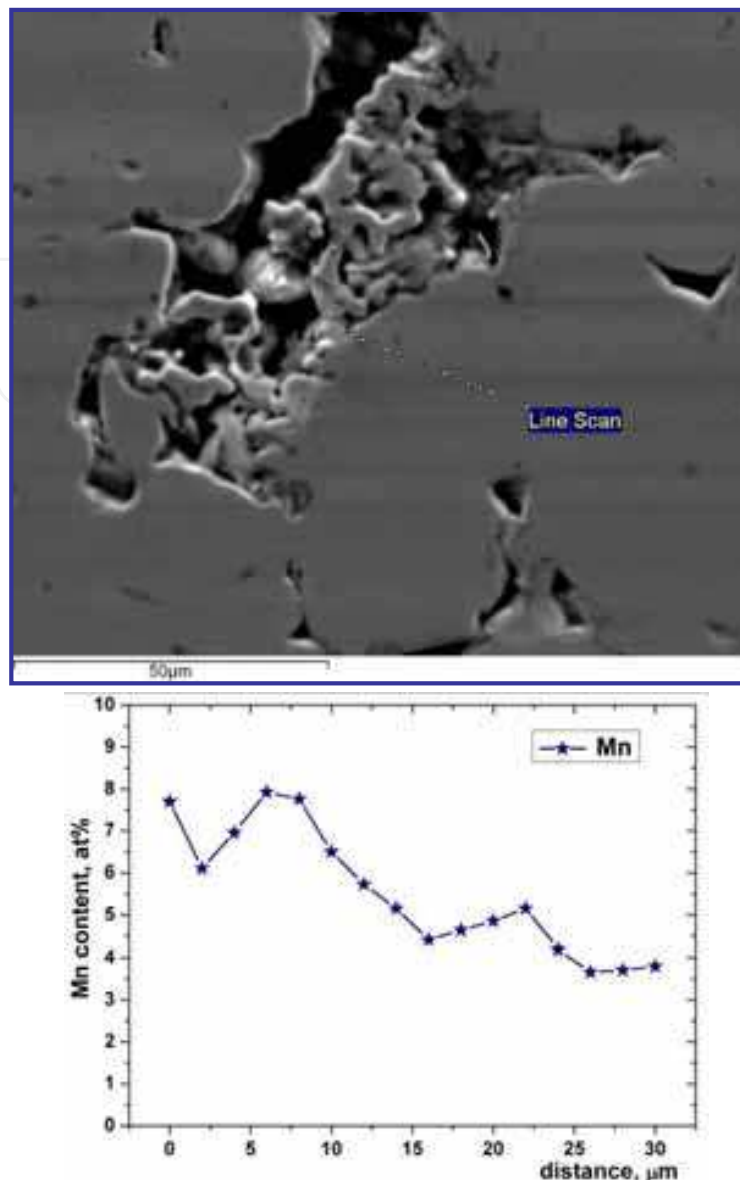
Fig. 11. SEI image of the area around ferromanganese residue for Fe-0.8Mn-0.5C specimen, sintered at 1120 °C for 30 min, with marked points of line Wave-length Dispersive X-ray analysis and results of manganese distribution

More detailed study of the iron-zinc system by Chongmo (Chongmo&Hillert, 1981), indicate formation of fine-grained zinc-rich surface layer on the initial stage of alloying. These fine grains reveal fast growth with increasing heat-treatment time and temperature and disappear rather fast. However, such fine-grained structure is much more difficult to observe by conventional metallography in the Fe-Mn powder system due to the difficulties of specimens preparation (porous and very heterogeneous structure). Nevertheless, such a fine-grain structure around manganese carrier residues was confirmed recently by (Hryha, 2007) by careful analysis of the fracture surface around manganese carrier residue using high-resolution scanning electron microscopy. Example of such fine-grained structure around manganese carrier particle is presented in Fig.12. Metallographic observation of the same material do not allow to clearly distinguish fine-grained structure of manganese-enriched area around ferromanganese residue in neither un-etched nor in etched state, see Fig.13. It is important to

note that most probably such fine-grained structure appears in this material at much lower
temperature, when the prerequisite for its formation – manganese evaporation/condensation
(after ~700°C) become more intensive. However, it is possible to observe only at higher
temperature (after ~1000°C) on the fracture surface because there are two main prerequisites of
its appearance on the fracture surface: grain boundaries of these fine grains has to be
weakened (degraded) and inter-particle necks around manganese carrier particles has to be
strong enough (stronger than inter-granular cohesion). Unlike in iron-zinc system, this fine
grained structure does not disappear with the temperature increasing and is observed even
after sintering at low temperature of 1120°C, see Fig.14. Moreover, after sintering at low
temperature, especially at unsatisfactory sintering atmosphere purity (dew point <-45°C), this
fine-grained structure is even more pronounced and can be even easily distinguished by
metallography, see Fig.14. High-temperature sintering at good conditions allows to avoid fine-
grained structure around manganese carriers. Degradation of grain boundaries of these fine
grains is very harmful to the mechanical properties of the admixed manganese-containing PM
steels, as it is described in next section. Metallographic evidence of fine-grained structure
around ferromanganese carrier particles after heating of Fe-3Mn-0.5C material to 1040°C was
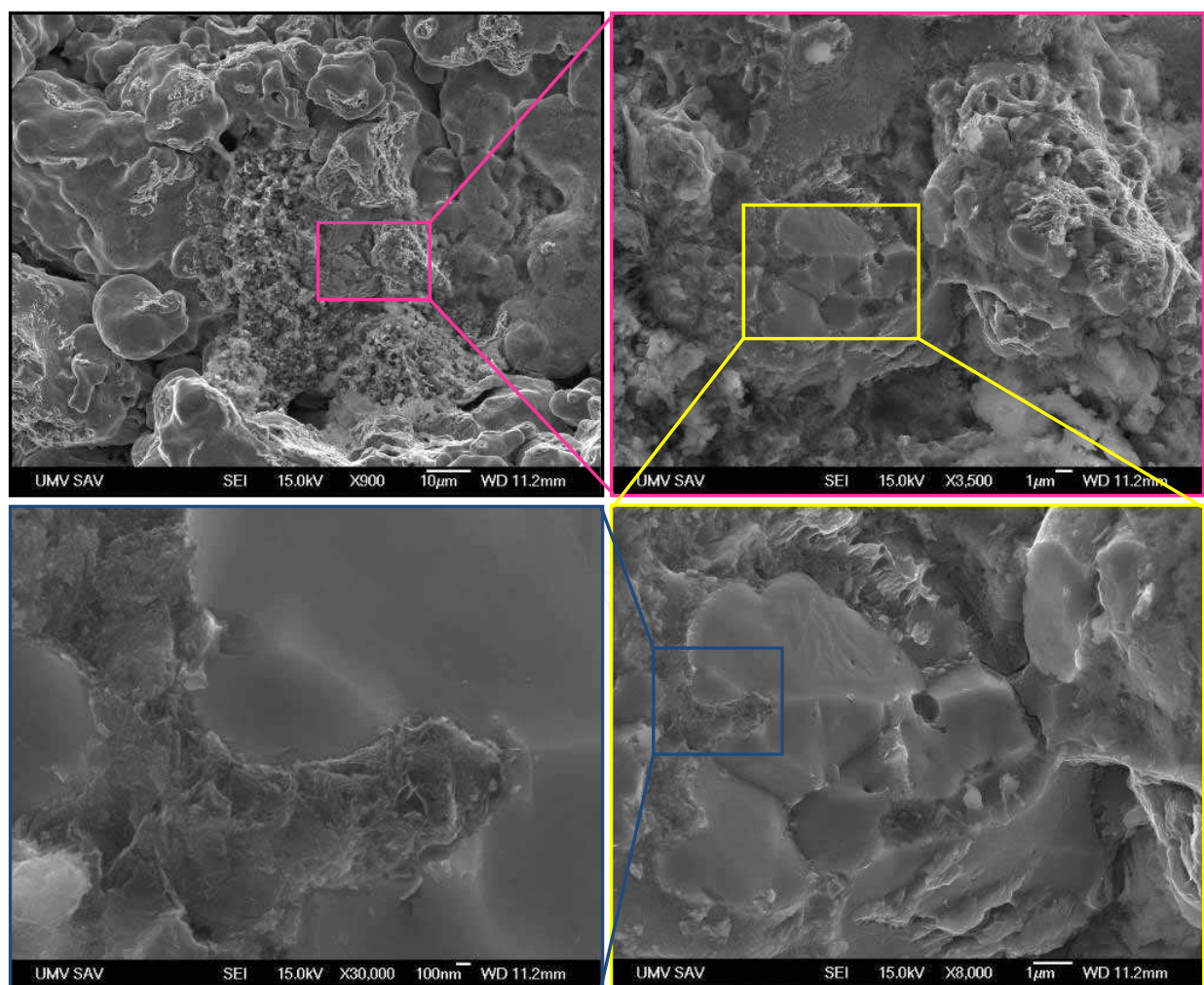revealed in the recent work of (Dudrova et al., 2010) by using specially designed etchant.

Fig. 12. Fine-grained structure of the manganese-reach surface layer around manganese
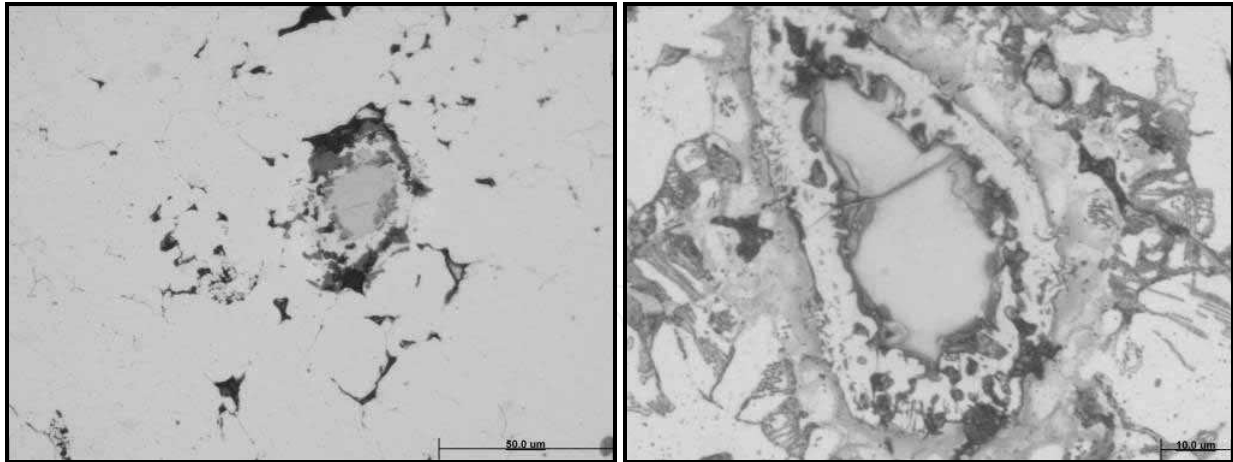carrier particle in Fe-0.8Mn-0.5C material, heated up to 1050°C (*Hryha, 2007*)

Fig. 13. Microstructure of Fe-0.8Mn-0.5C material, heated up to 1050°C in un-etched (left) and etched (right) state (*Hryha, 2007*)
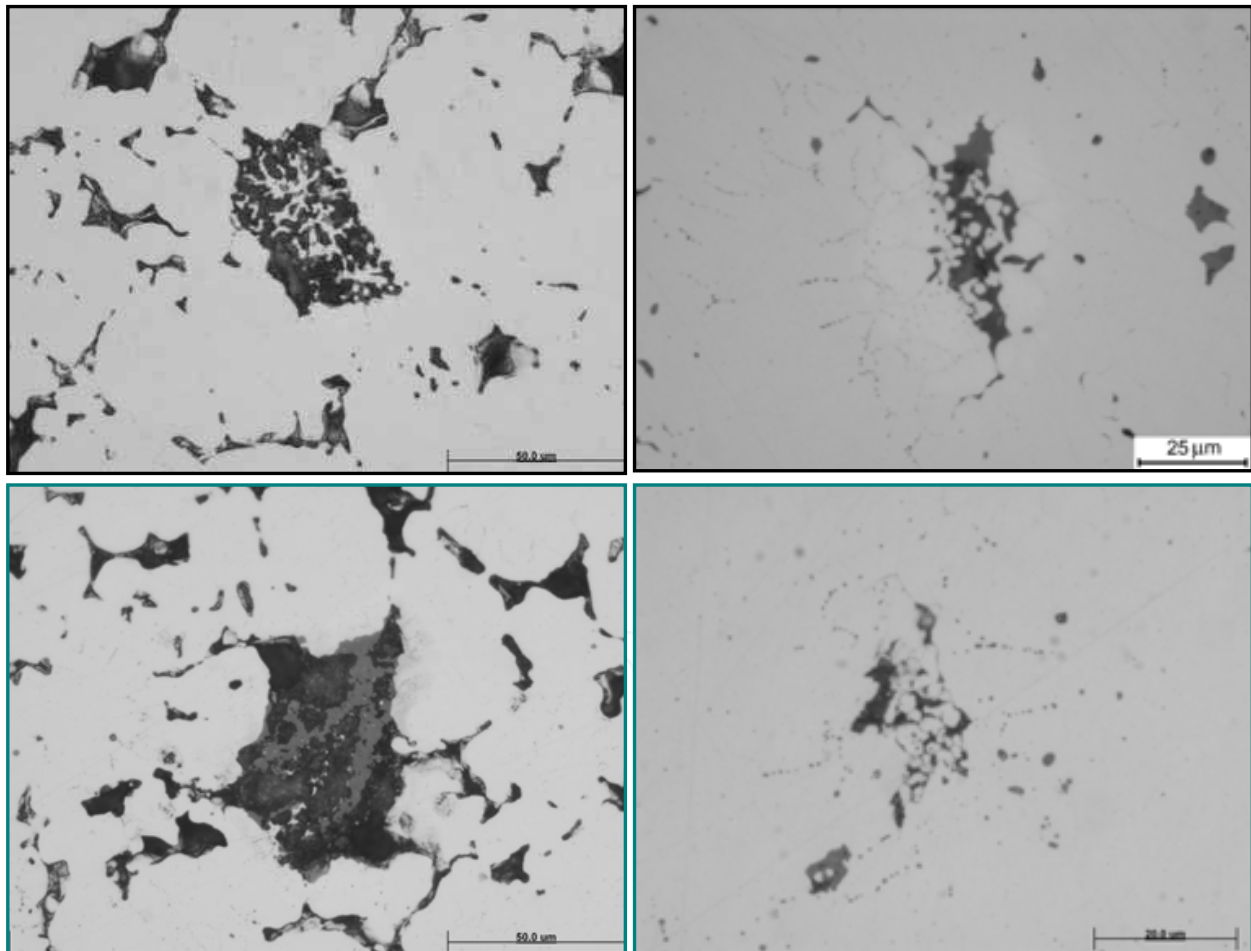

Fig. 14. Microstructure of Fe-0.8Mn-0.5C material, admixed with ferromanganese (upper row) and electrolytic manganese (bottom row), heated up to 1120°C (left) and after sintering at 1120°C for 30 min (right), showing network of 'point' oxides that mark fine grain structure around manganese carrier particles (*Hryha, 2007*)

5. Brittleness of admixed manganese containing PM steels

After about thirty years of an intensive investigation of the admixed manganese containing PM steels, number of inventions concerning adjustment of the sintering process and manganese carrier did not result in wide industrial application of mentioned above materials. The main obstacle for industrial application of admixed manganese PM steels is high brittleness of sintered components. Several hypotheses have been proposed, connected with brittleness caused by microstructure heterogeneity, size of manganese carrier particles, their residue and their oxidation (Dudrova et al., 2004; Dudrova et al., 2005; Danninger et al., 2005; Cias et al., 2003).

5.1 Effect of manganese carrier residues.

Detrimental effect of pores, filled with slag, after manganese source due to its evaporation was emphasized by Dudrova (Dudrova et al., 2004) and Danninger (Danninger et al., 2005). Due to angular shape of such pores with inclusions they act as strong crack-initiation sites. High-temperature sintering leads to rather significant reduction of slag, preferably formed by thermodynamically stable complex oxides, and pore rounding, however it did not result in so considerable mechanical properties improvement as it was expected.

Appearance of electrolytic manganese and ferromanganese residues after heating up to 1120°C, presented in Fig. 15, reveal some differences in the residues appearance and composition. Ferromanganese residue has complex porous shape with the presence of phase on the surface of the pore with smooth surface and numerous cracks, pointing to presence of liquid phase at this temperature. Formation of the liquid phase is thermodynamically probable at this temperature in the wide range of concentration in the Fe-Mn-C system, see Fig.5, taking into account manganese evaporation and diffusion of iron and carbon into manganese carrier particle. Residues of electrolytic manganese particles have a shape of contamination agglomerate, formed by manganese oxide with traces of manganese sulphide. Residues of ferromanganese have more complex chemical composition due to higher amount of silicon oxide in it (Hryha, 2007).
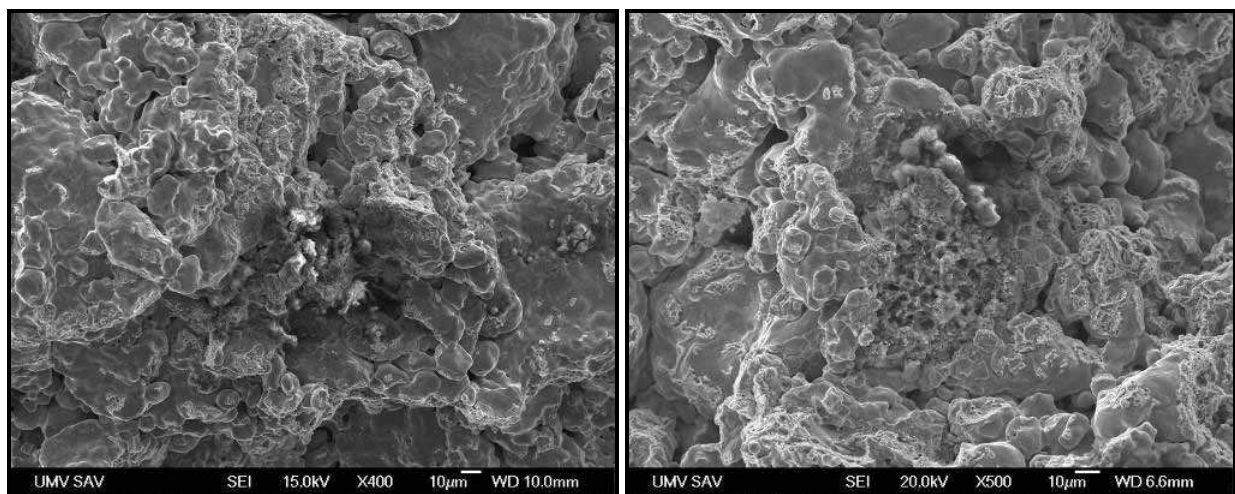

Fig. 15. Appearance of manganese carrier residue after heating to 1120°C in the case of Fe-0.8Mn-0.5C material, admixed with electrolytic manganese (left) and ferromanganese (right) (*Hryha, 2007*)
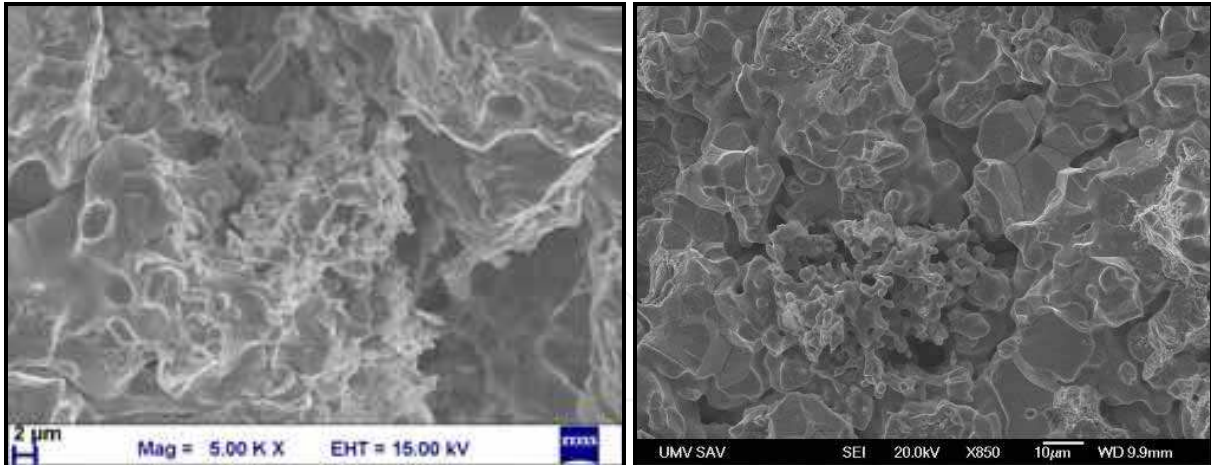
Fig. 16. Appearance of manganese carrier residue after sintering at 1120°C for 30 min in the case of Fe-0.8Mn-0.5C material, admixed with electrolytic manganese (left) and ferromanganese (right)
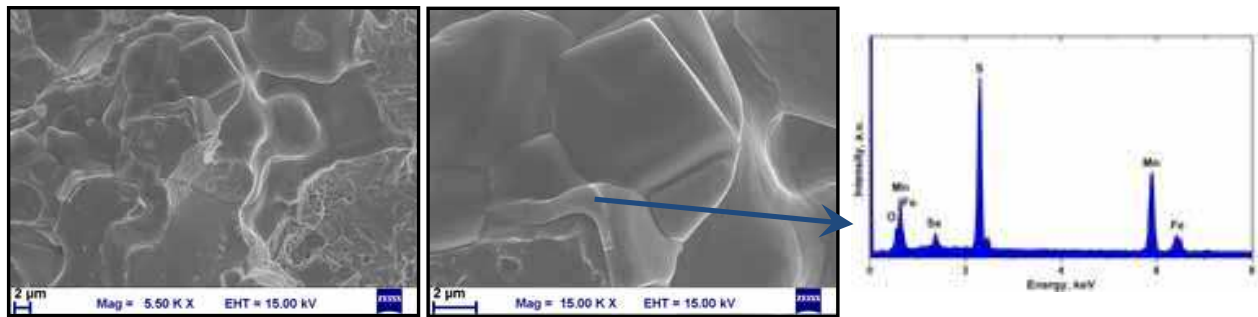

Fig. 17. SEM+EDX analysis of the electrolytic manganese residue after sintering at 1200°C for 30 min on the fracture surface of Fe-0.8Mn-0.5C material
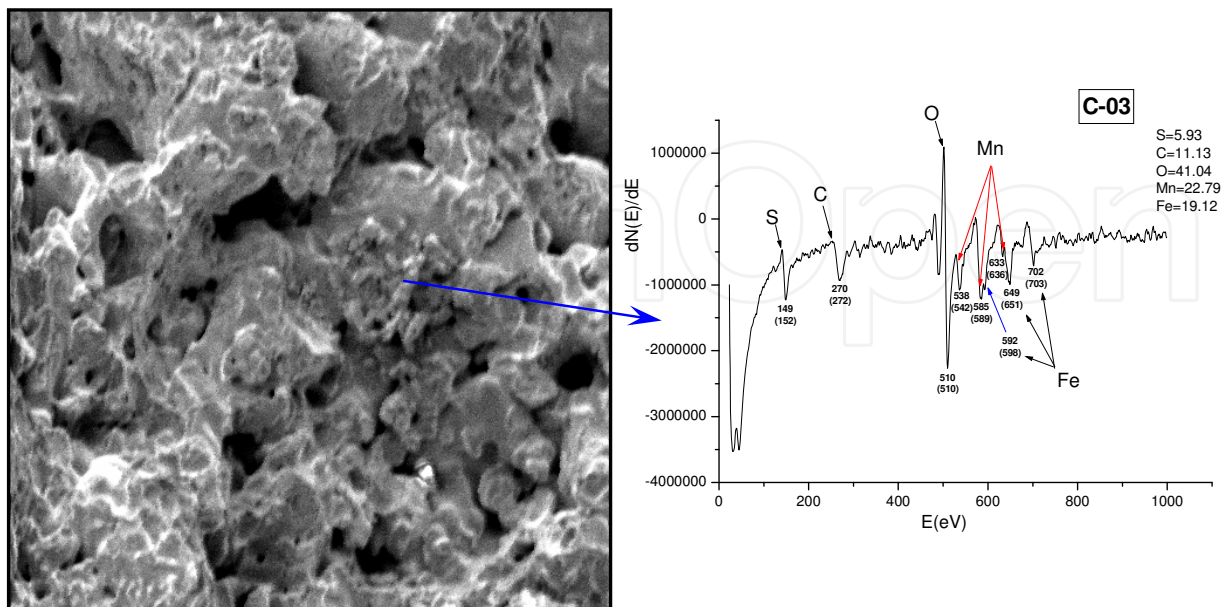

Fig. 18. Auger spectra of the ferromanganese residue after sintering at 1120°C for 30 min on the fracture surface of Fe-0.8Mn-0.5C material

Sintering even at 1120ºC for 30 min in good atmosphere purity allows considerable reduction of manganese carrier residues in size and amount of manganese oxide as well as morphology change, see Fig.16. Residue of electrolytic manganese looks more like inclusion agglomerate, whereas ferromanganese residue has specific 'coral-like'-shape. According to the results of SEM+EDX and Auger analyses, see Figs.17 and 18, in both cases residua are composed of manganese oxide with larger amount of manganese sulphide, than it was observed before sinter-holding. However after sintering at high-temperature (1200ºC) together with essential decrease in size of the manganese residues the oxygen content decreases as well, while much higher sulphur content is registered. Ferromanganese residue also contain large amount of silicon oxide.

5.2 Inter-granular decohesion brittleness.

Application of high-purity sintering atmospheres combined with high-temperature sintering and utilization of fine manganese carrier powder will considerably minimize detrimental effect of large angular pores on the mechanical properties. However, careful examination of the areas around manganese carrier particles at high magnification reveal more critical defect, presented in the admixed manganese systems. Recent studies of brittleness of admixed with manganese PM steels studied by complex of advanced microscopy and spectroscopy techniques (high-resolution scanning electron microscopy (HR SEM), energy dispersive X-ray analysis (EDX), Auger spectroscopy and X-ray photoelectron spectroscopy (XPS)) clearly indicate that the brittleness of material containing admixed manganese is caused by the weakness of grain boundaries within the base matrix particles around the manganese carrier residuals (Hryha, 2007; Hryha et al., 2008; Hryha et al., 2010). Completely brittle behaviour associated with predominantly inter-granular type of failure caused by the oxide phase at grain boundaries was also assumed in previous works by Dudrova (Dudrova et al., 2004; Dudrova et al., 2005).

Inter-granular type of failure starts to be observed in the admixed materials above ~1000ºC, see Fig.12, caused by the presence of very thin manganese oxide layer, formed due to diffusion of condensed manganese from the iron particle surface inside the particles along the grain boundaries and its further oxidation there. However, inter-granular type of failure around manganese carrier residua is much better pronounced after low-temperature sintering, see Fig.19. Large number of fine point inclusions (size <200 nm) can be seen on the inter-granular decohesion facets, that according to SEM+EDX analysis are formed preferably by manganese oxides after sintering at 1120ºC, see Fig.20.

These point oxides on the degraded grain boundaries around manganese residuals are evident on the unetched microstructure of admixed materials, see Fig.14, forming on metallographic cut ''chains'' of point oxides. They develop close to the sintering temperature and are much better pronounced after sintering at 1120ºC for 30 min. The networks of point oxides are better pronounced for materials admixed with electrolytic manganese.

Presence of these point inclusions on the grain-boundaries around manganese carrier residues explains why this fine grain structure does not disappear with temperature increasing or after sintering at low temperature, as it can be expected based on behaviour of iron-zinc system with similar dissolution of zinc by DIGM mechanism. Large amount of point oxides hamper grain growth of fine manganese-enriched grains, formed around

manganese carrier source. Sintering at lower atmosphere purity leads to increased amount of inter-granular decohesion facets with higher amount of point oxides on them. This is also reflected on higher microstructure heterogeneity due to the retarded manganese dissolution caused by hampering grain boundary motion by point oxides.
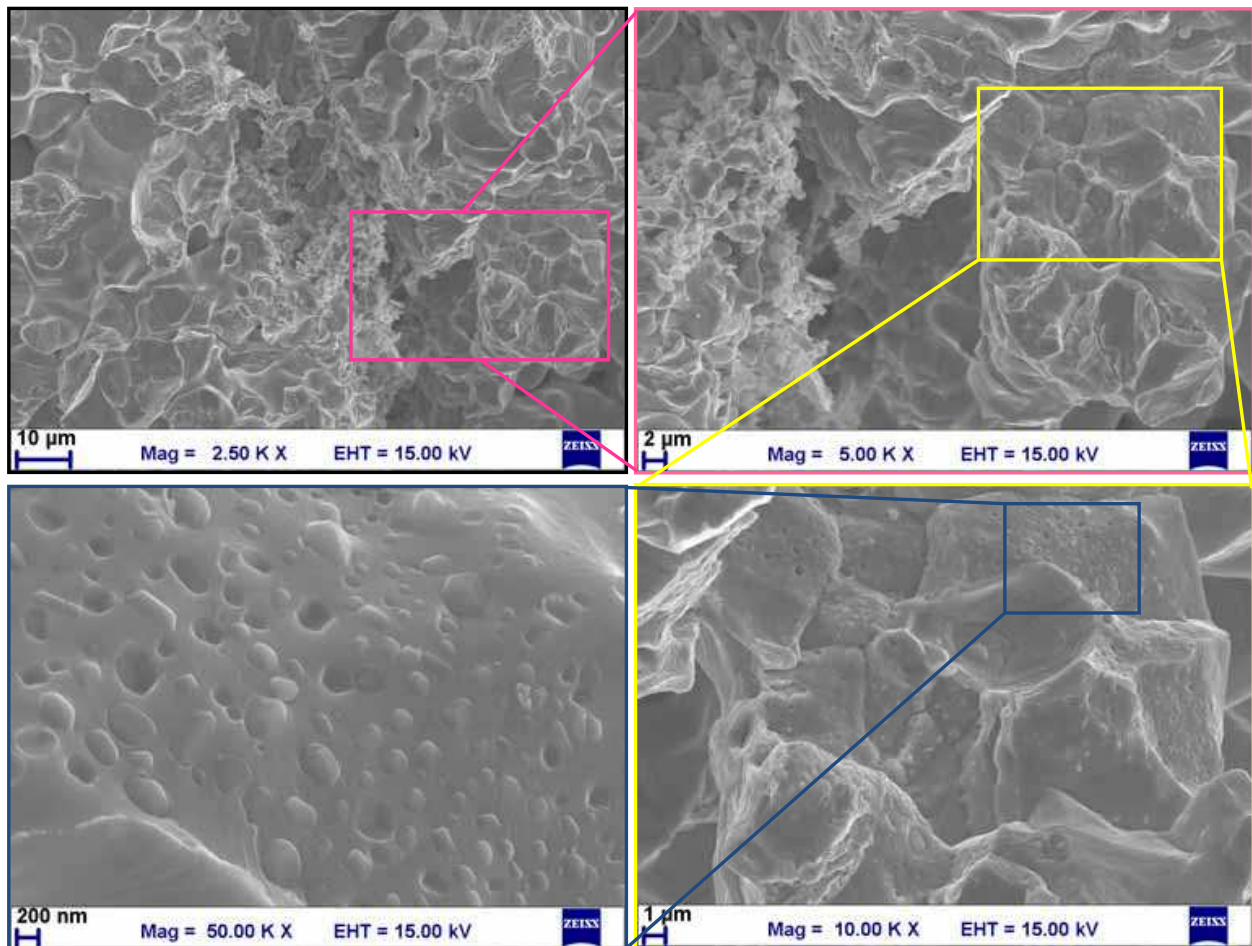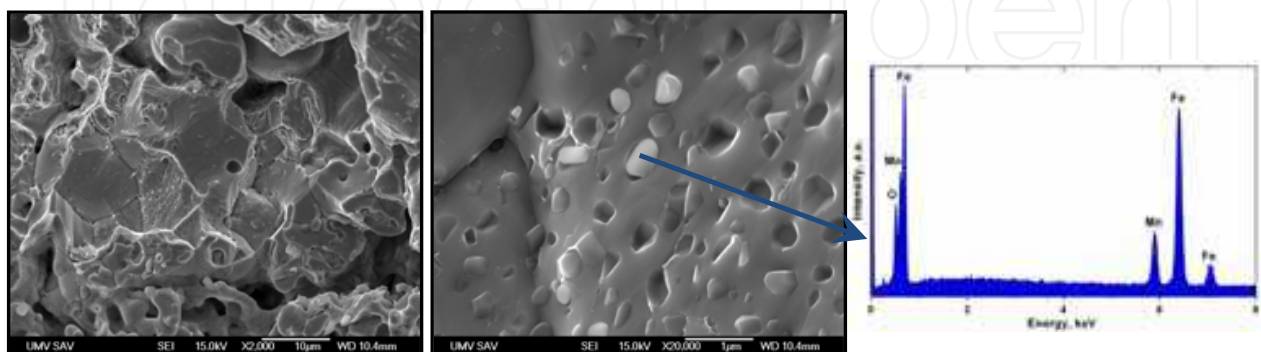

Fig. 19. Inter-granular decohesion facets around electrolytic manganese residue after sintering at 1120°C for 30 min on the fracture surface of Fe-0.8Mn-0.5C material

Fig. 20. SEM+EDX analysis of particulate inclusions on the inter-granular decohesion facets around ferromanganese residue after sintering at 1120°C for 30 min on the fracture surface of Fe-0.8Mn-0.5C material

Due to the lower amount of point oxides on the degraded grain boundaries at lower temperatures, such residual inter-granular brittleness is nearly fully removed for material admixed with ferromanganese after high-temperature sintering, see Fig.21, but is still observed for admixed with electrolytic manganese material.
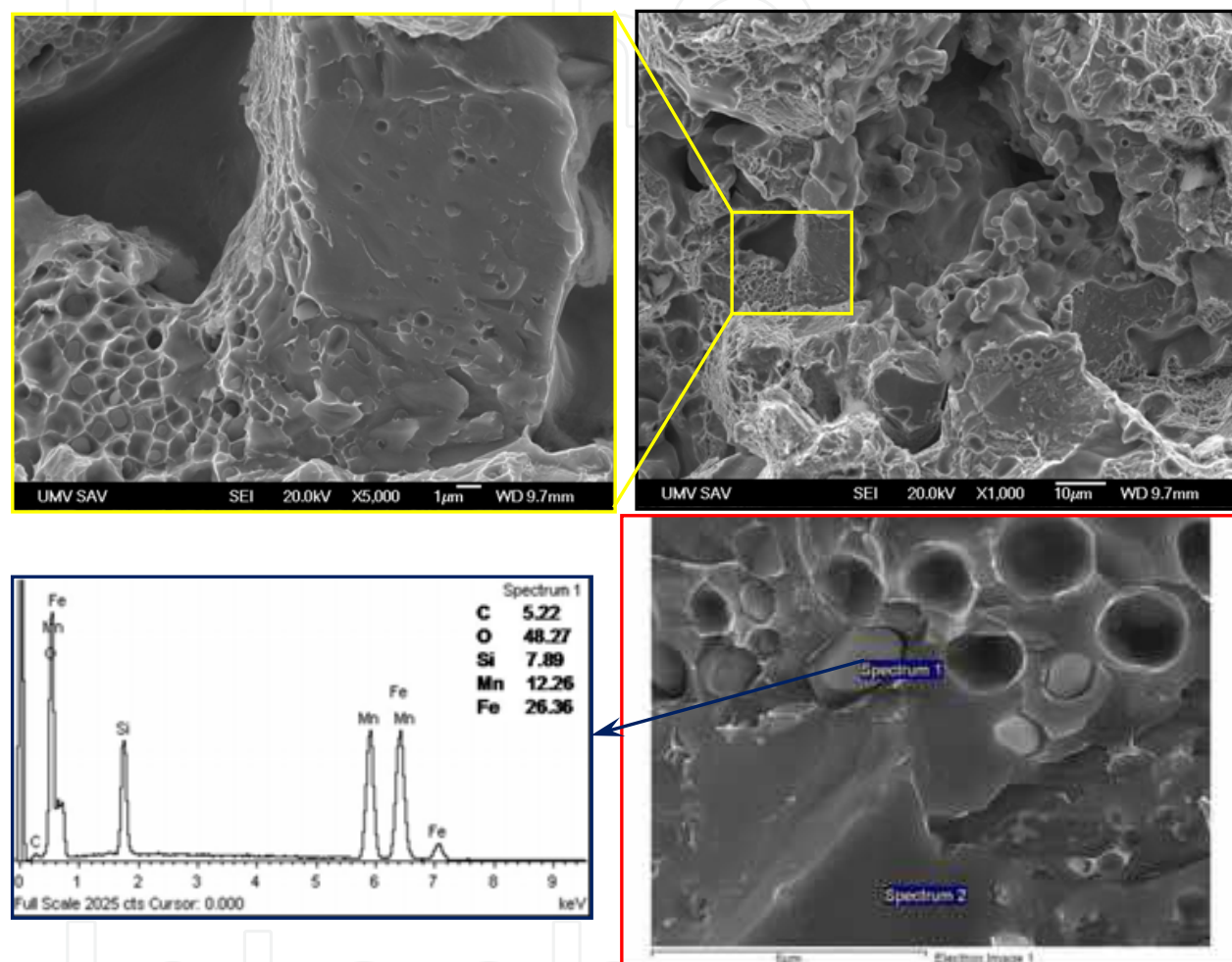

Fig. 21. SEM+EDX analysis of particulate inclusions on the inter-granular decohesion facets around ferromanganese residue after sintering at 1200°C for 30 min on the fracture surface of Fe-0.8Mn-0.5C material

Results of XPS analysis confirm presence of manganese oxides and sulphides on the fracture surface of both admixed specimens even after high-temperature sintering, see Fig.22 (Hryha et al., 2008; Hryha et al., 2010-b). The analyses also indicate that there is no significant difference in surface composition between the two admixed alloys. The XPS analyses show higher amount of oxides/sulphides present on the fracture surface of admixed with ferromanganese material due to larger ferromanganese residues after high-temperature sintering.
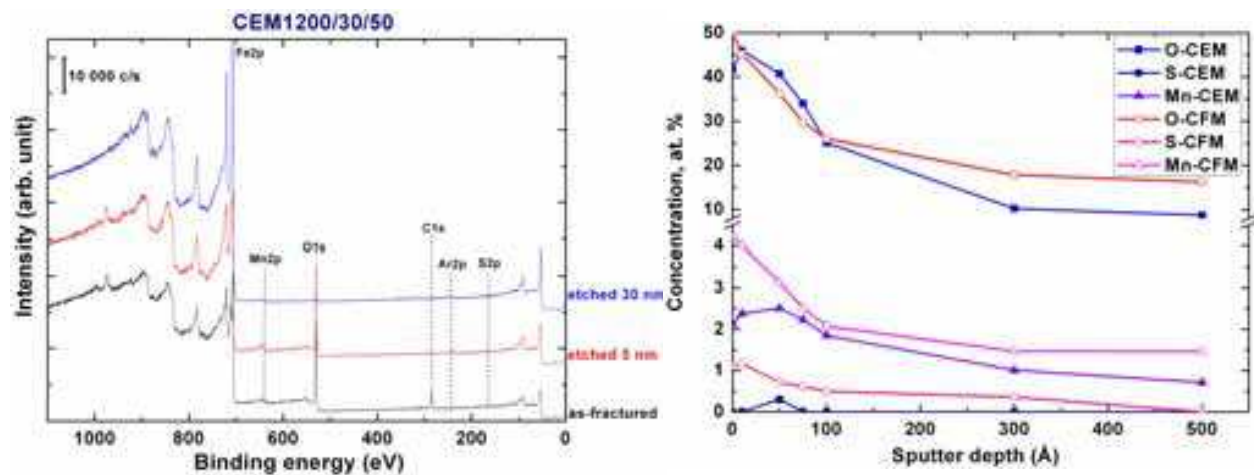
Fig. 22. XPS survey scan of fracture surface of admixed with electrolytic manganese Fe-0.8Mn-0.5C material (left) and comparison of elements concentration profile (right) for admixed with electrolytic (**CEM 1200/30)** and ferromanganese **(CFM 1200/30)** materials, sintered at1200°C for 30 min

6. Effect of alloying mode

Summarizing the results of number of investigation performed up to now, it is clear that admixed materials are exposed to considerable oxidation during heating stage even when applying high purity sintering atmospheres. Sintering at lower atmosphere purity without hydrogen presence results in even higher oxidation of admixed alloys (Hryha, 2007). Comparison of oxygen content and mass-gain reveals highest oxidation of admixed with electrolytic manganese alloy and lowest oxidation in the case of prealloyed material (Hryha, 2007; Hryha et al., 2010-b). In addition temperature ranges of considerable oxidation of admixed alloys coincides with the onset of intensive manganese sublimation (>720°C), pointing out that these processes are closely related and are connected with the oxidation of manganese carrier particles.

This can be shortly described by a model of evolution of manganese carrier particles, describing manganese sublimation and further oxidation of Mn vapour and its influence on the oxides distribution and development of inter-particle connections in the areas adjoining to manganese carrier, presented in Fig.23. During first stages of heating manganese carrier particle is naturally oxidized and is covered by thick oxide layer (Fig.23 (a)). After 700°C, when manganese starts to sublimate, Mn vapour reacts with oxygen presented in sintering atmosphere, water vapour and carbon oxides (produced by reduction of iron oxide layer). Formed manganese oxide condenses on the surface of the iron particles, adjoining to manganese source. Temperature increasing leads to reduction of iron oxides and starting of the inter-particle necks development and, at the same time, more intensive manganese evaporation and distribution through the pore system, its further oxidation and formation of Mn-oxide layer on the adjoining pores, see Fig.23 (b) – red areas. This stage can be characterized as 'shift' of oxidation – oxygen from the iron oxide from the base powder is transformed to manganese oxide around manganese carrier particles, that coincides with the keeping of the same level of oxygen content during heating for both admixed systems (Hryha et al., 2010-b). The problem with such manganese oxide layer is that it obstructs formation of metal-metal contacts between base powder particles and so development
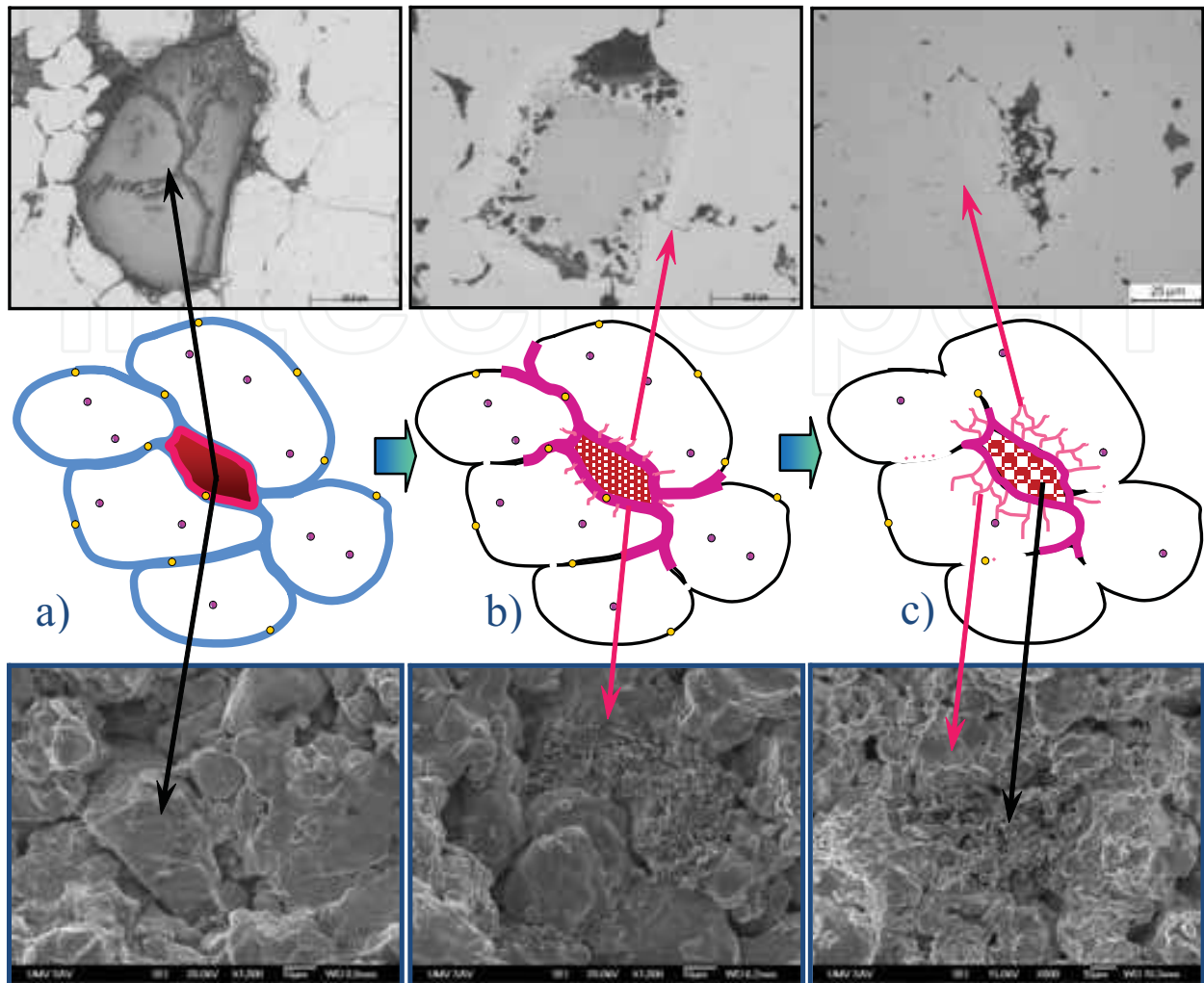
Fig. 23. Model of the evolution of the manganese carrier particles and inter-particle
connections around them from 720°C (left), 1000°C (middle) to as-sintered structure
(1120°C/30 min)

of inter-particle connections, that are formed only on the larger distance from Mn-carriers,
see Fig.23 (b). The extension of such contaminated region is bigger for admixed with
electrolytic manganese material and is increasing with temperature – at 1000°C it reaches
around 100 µm, depending on surrounding pores structure. Lower total amount of the inter-
particle connections is reflected in much lower strength values during heating stage,
especially for admixed with electrolytic manganese material, see Fig.24. Temperature
increasing leads to improvement in local conditions inside pores that enable reduction of
surface manganese oxides and leads to decrease in size of contaminated areas. This enables
intensive growth of inter-particle connections around manganese source, see Fig.23 (c), and
is reflected on the increasing of the macro-strength of compact between 1000 and 1120°C, see
Fig.24. It is important to emphasize that even after sintering at 1120°C properties of admixed
with electrolytic manganese material (strength and oxygen content) are inferior in
comparison with admixed with ferromanganese material, that now is close to the prealloyed
material and only after sintering at 1200°C improvement in properties of admixed with
electrolytic manganese material can be seen. This is connected with the slower reduction of

manganese oxides, enclosed inside inter-particle necks and formed on the grain-boundaries during manganese dissolution. Presence of manganese carrier particles during the whole heating stage is another confirmation of their intensive oxidation – presence of the thick oxide layer retard intensive manganese evaporation during heating stage.
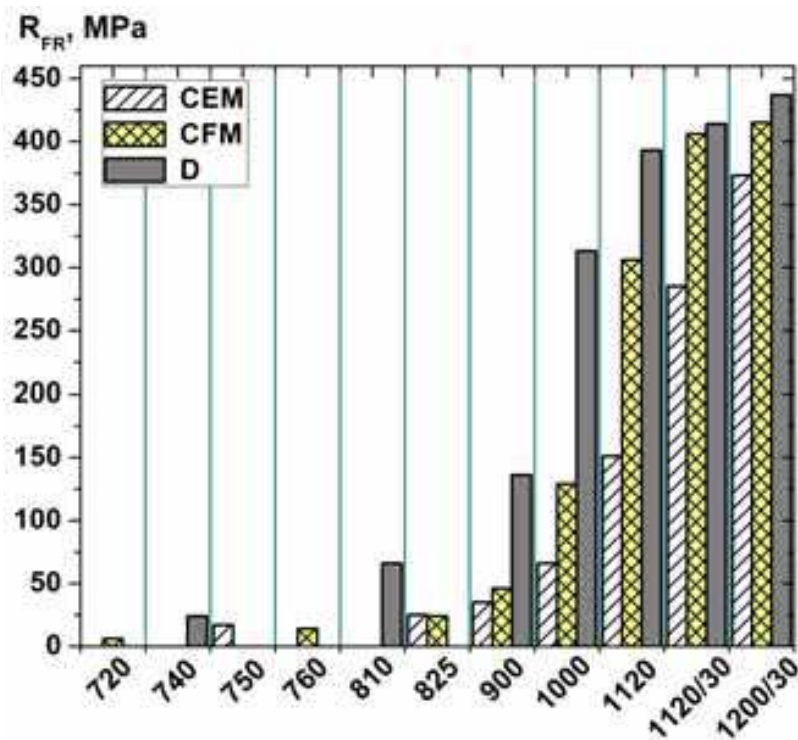

Fig. 24. Rupture strength of interrupted sintered specimens of Fe-0.8Mn-0.5C material, based on admixed with electrolytic manganese (CEM) and ferromanganese (CFM) systems as well as fully prealloyed powder (D), (*Hryha et al., 2010-b*)

7. Summary

Detailed analysis of manganese containing sintered steels based on fully prealloyed powder and admixed systems using high-purity electrolytic manganese and medium-carbon ferromanganese, indicate high brittleness of admixed materials. Lower strength of admixed materials is described based on oxidation of manganese vapor and its further condensation on the surrounding iron particles that suppress inter-particle necks development in the areas around the manganese source and results in extended defect areas. The worst results were obtained for admixed with electrolytic manganese material that is explained by more intensive manganese evaporation and accordingly higher specimen oxidation at low temperatures. Second type of critical defects in admixed systems is connected with the degradation of grain-boundaries around manganese carrier particles due to the presence of complex oxides and manganese sulfide on the inter-granular decohesion facets. The amount and composition of the contaminants after sintering are determined by the type of manganese carrier used and sintering conditions.

Number of presented in literature experimental results indicates that it is no doubt that the observed depth of manganese alloyed areas around manganese carrier particles is much

larger than volume diffusion could account for. Recent author's experimental results clearly show that much higher diffusivity observed can be described only based on complex mechanism – combination of grain boundary diffusion and chemically induced grain boundary migration (DIGM). Alloying mechanism with the presence of the gas phase (manganese vapour) and fine-grained structure of the manganese-rich surface layer on the initial stage of alloying abundantly evidences validity of this hypothesis.

Utilization of hydrogen-containing atmospheres of high-purity and higher heating rate at medium temperatures range (700-1000°C) together with sintering at high temperatures (≥1200°C) are suggested for successful sintering of admixed with manganese PM steels. Lower sensitivity to atmosphere purity, homogeneously distributed microstructure, absence of the large contaminated pores and oxide inclusions indicate definite advantage of pre-alloyed powder system from both economical and technical points of view.

8. Future research

Availability of new thermodynamic data concerning low-melting point systems and application of modern sintering techniques for high-temperature sintering combined with advanced control of sintering atmosphere open space for development of new master-alloys based on Fe-Mn-C systems. During design of such master-alloys stress has to be set on homogenisation and alloying through transient liquid phase and shifting manganese evaporation to as high temperatures as possible otherwise intensive formation of stable manganese oxide is unavoidable. Improved diffusivity of manganese by DIGM mechanism is another strong side of utilization of admixed iron-manganese PM steels. However, recent study (Hryha et al., 2010-a) shows high quality of the manganese prealloyed powder from the surface composition point of view that allow us to expect the appearance of manganese alloyed steel powder on the market in near future.

9. Acknowledgement

10. References

Beiss, P. (2006). Alloy Cost Optimization of High Strength Mn-Cr-Mo Steels with Kerosene-Atomized Master Alloy. *Advances in Powder Metallurgy and Particulate Materials-2006*, pp. 727-735, ISSN: 1065-5824, San Diego, CA, June 2006, MPIF.

Chongmo, L. & Hillert, M. (1981). A Metallographic Study of Diffusion-Induced Grain Boundary Migration in the Fe-Zn System. *Acta Metallurgica*, Vol. 29, (1981), pp. 1949-1960, ISSN: 0956-7151.

Cias, A.; Mitchell, S.C.; Watts, A. & Wronski, A.S. (1999). Microstructure and Mechanical Properties of Sintered (2-4)Mn-(0.6-0.8)C Steels. *Powder Metallurgy*, Vol. 42, (1999), pp. 227-233, ISSN (printed): 0032-5899. ISSN (electronic): 1743-2901.

Cias, A.; Mitchell, S.C.; Plich, K., Cias, H.; Sulovski, M. & Wronski, A.S. (2003). Tensile Properties of Fe-3Mn-0.6/0.7C Steels Sintered in Semiclosed Containers in Dry Hydrogen, Nitrogen and Mixtures thereof. *Powder Metallurgy*, Vol. 46, (2003), pp. 165-170, ISSN (printed): 0032-5899. ISSN (electronic): 1743-2901.

Cias, A. & Wronski A.S. (2008). Comparison of Mechanical Poperties of Manganese Steels of the Same Chemical Composition Based on Sponge and Atomised Iron Powders. *Powder Metallurgy Progress*, Vol. 8, No. 2, (2008), pp. 76-82, ISSN: 1335-8987.

Danninger, H.; Gierl, C.; Kremel, S.; Leitner, G.; Jaenicke-Roessler, K. & Yu, Y. (2002). Degassing and Deoxidation Processes During Sintering of Unalloyed and Alloyed PM Steels. *Powder Metallurgy Progress*, Vol. 2, No. 3, (2002), pp. 125-139, ISSN: 1335-8987.

Danninger, H.; Pöttschcher, R.; Bradac, S.; Šalak, A & Seykammer, J. (2005). Comparison of Mn, Cr and Mo alloyed sintered steels prepared from elemental powders. *Powder Metallurgy*, Vol. 48, (2005), pp. 23-32, ISSN (printed): 0032-5899. ISSN (electronic): 1743-2901.

Dudrova, E.; Kabatova, M.; Bidulsky, R. & Wronski, A.S. (2004). Industrial Processing, Microstructures and Mechanical Properties of Fe-(2-4)Mn-0.85Mo-(0.3-0.7)C Sintered Steels. *Powder Metallurgy*, Vol. 47, (2004), pp. 181-190, ISSN (printed): 0032-5899. ISSN (electronic): 1743-2901.

Dudrova, E.; Kabatova, M.; Bures, R.; Bidulsky, R. & Wronski, A.S. (2005). Processing, Microstructure and properties of 2–4%Mn and 0.3/0.7%C sintered steels. *Kovové materiály /Metallic Materials*, Vol. 43, (2005), pp. 404-421, ISSN: 0023-432X.

Dudrova, E.; Kabatova, M.; Mitchell, S.C.; Bidulsky, R. & Wronski, A.S. (2010). Microstructure Evolution in Fe-Mn-C during Sintering. *Powder Metallurgy*, Vol.53, No.3, (2010), pp.244-250, ISSN (printed): 0032-5899. ISSN (electronic): 1743-2901.

Gaskell, D.R. (2003). *Introduction to the Thermodynamics of Materials*, 4-th ed., Taylor&Francis, Publisher, ISBN 1-56032-992-0, New York, 2003, 618 p.

Gomez-Acebo, M.; Sarasola, M. & Castro, F. (2003). Systematic Search of Low Melting Point Alloys in the Fe-Cr-Mn-Mo-C System. *Computer Coupling of Phase Diagrams and Thermochemistry*, Vol. 27, (2003), pp. 325-334, ISSN: 0364-5916.

Hillert, M. & Purdy, G.R. (1978). Chemically Induced Grain Boundary Migration. *Acta Metallurgica*, Vol. 26, (1978), pp. 333-340, ISSN: 0956-7151.

Hoffmann, G. & Dalal, K. (1979). Development and Present Situation of Low Alloyed PM Steels Using MCM and MVM Master Alloys. *Powder Metallurgy International*, Vol. 11, (1979), pp. 177-180, ISSN: 0048-5012.

Hryha, E. & Dudrova, E. (2007). The Sintering Behaviour of Fe-Mn-C Powder System, Correlation between Thermodynamics and Sintering Process, Mn Distribution, Microstructure. *Materials Science Forum*, Vol.534-536, (2007), pp. 761-764, ISSN: 0255-5476.

Hryha, E. (2007). Fundamental Study of Mn Containing PM Steels with Alloying Method of both Premix and Pre-alloy. *PhD Thesis*, (2007), 257 p., IMR SAS, Kosice, Slovakia.

Hryha, E.; Nyborg, L.; Dudrova, E. & Bengtsson, S. (2008). Brittleness of Structural PM Steels Admixed with Manganese Studied by Advanced Electron Microscopy and Spectroscopy. *Powder Metallurgy Progress*, Vol. 8, No. 2, (2008), pp. 109-114, ISSN: 1335-8987.

Hryha, E.; Nyborg, L.; Dudrova, E. & Bengtsson, S. (2009-a). Microstructure Development
during Sintering of Manganese Alloyed PM Steels. *Proceedings of International
Powder Metallurgy Congress & Exhibition Euro PM2009*, Vol. 1, pp. 17-22, ISBN
9781899072064, Copenhagen, Denmark, October 2009, EPMA, Shrewsbury, UK.

Hryha, E.; Nyborg, L. & Bengtsson, S. (2009-b). Surface Analysis of Prealloyed with
Manganese Steel Powder. *Proceedings of International Powder Metallurgy Congress &
Exhibition Euro PM2009*, Vol. 2, pp. 169-174, ISBN 9781899072071, Copenhagen,
Denmark, October 2009, EPMA, Shrewsbury, UK.

Hryha, E.; Girl. C.; Nyborg, L.; Danninger, D. & Dudrova, E. (2010-a). Surface Composition
of the Steel Powders Pre-Alloyed with Manganese. *Applied Surface Science*, Vol. 256,
No. 12, (2010), pp. 3946-3961, ISSN: 0169-4332.

Hryha, E.; Nyborg, L. & Dudrova, E. (2010-b). Critical Aspects of Alloying of Sintered Steels
with Manganese. *Metallurgical and Materials Transaction A*, Vol. 41A, No.11, (2010),
pp. 2880-2897, ISSN: 1073-5623.

Mitchell, S.C. & Cias, A. (2004). Carbothermic Reduction of Oxides During Nitrogen
Sintering of Manganese and Chromium Steels. *Powder Metallurgy Progress*, Vol. 4,
No. 3, (2004), pp. 132-142, ISSN: 1335-8987.

Navara, E. (1982). Alloying of Sintered Steels with Manganese. *Proceedings of VI-th
International Conference on Powder Metallurgy*, Vol. 1, pp. 143-154, Brno, Czech
Republic, 1982, EPMA, Shrewsbury, UK.

Nohara, K. & Hirano, K. (1971). Diffusion of Mn in Fe and Fe-Mn Alloys. *Suppl. Trans. Iron
Steel Jpn.*, Vol. 11, (1971), pp. 1267-1273, ISSN: .

Sainz, S.; Martinez, V.; Dougan, M.; Baumgaertner, F. & Castro, F. (2006). Sinterability,
Hardenability and Mechanical Properties of Mn-Containing PM Steels through the
Use of a Specially Designed Fe-Mn-C Master Alloy. *Advances in Powder Metallurgy
and Particulate Materials-2006*, pp. 624-637, ISSN: 1065-5824, San Diego, CA, June
2006, MPIF.

Schlieper, G. & Thummler, F. (1979). High Strength Heat-Treatable Sintered Steels
Containing Manganese, Chromium, Vanadium and Molybdenum. *Powder
Metallurgy International*, Vol. 11, (1979), pp. 172-176, ISSN: 0048-5012.

Šalak, A. (1980-a). Sintered Manganese Steels, Part II: Manganese Evaporation During
Sintering. *Powder Metallurgy International*, Vol. 12, (1980), pp. 72-75, ISSN: 0048-
5012.

Šalak, A. (1980-b). Manganese Sublimation and Carbon Ferromanganese Liquid Phase
Formation During Sintering of Premixed Manganese Steels. *The International Journal
of Powder Metallurgy and Powder Technology*, Vol. 16, No.4, (1980), pp. 369-379, ISSN:
0361-3488.

Šalak, A. (1989). Diffusion Induced Grain Boundary Migration by Iron Powder Alloying by
Manganese Vapour. *Kovové materiály / Metallic Materials*, Vol. 27, No.2, (1989), pp.
159-170, ISSN: 0023-432X.

Šalak, A; Selecka, M. & Bureš, R. (2001). Manganese in Ferrous Powder Metallurgy. *Powder
Metallurgy Progress*, Vol. 1, No. 1, (2001), pp. 41-58, ISSN: 1335-8987.

Wells, C. & Mehl, R.F. (1941). Rate of Diffusion of Manganese in Gamma Iron in Low-carbon
and High-carbon Manganese Steels. *Trans. Am. Inst. Min. Met. Pet. Eng.*, Vol. 145,
(1941), pp. 315-328, ISSN: .

Zapf, G.; Hoffmann, G. & Dalal, K. (1975). Effect of Additional Alloying Elements on the Properties of Sintered Manganese Steels. *Powder Metallurgy*, Vol. 18, (1975), pp. 214-236, ISSN (printed): 0032-5899. ISSN (electronic): 1743-2901.
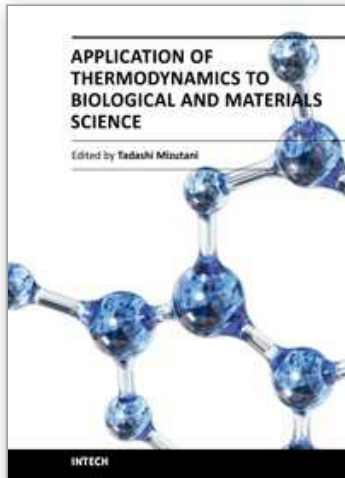
Application of Thermodynamics to Biological and Materials Science

Edited by Prof. Mizutani Tadashi

Progress of thermodynamics has been stimulated by the findings of a variety of fields of science and technology. The principles of thermodynamics are so general that the application is widespread to such fields as solid state physics, chemistry, biology, astronomical science, materials science, and chemical engineering. The contents of this book should be of help to many scientists and engineers.

How to reference

In order to correctly reference this scholarly work, feel free to copy and paste the following:

Eduard Hryha and Eva Dudrova (2011). The Sintering Behaviour of Fe-Mn-C Powder System, Correlation between Thermodynamics and Sintering Process, Manganese Distribution and Microstructure Composition, Effect of Alloying Mode, Application of Thermodynamics to Biological and Materials Science, Prof. Mizutani Tadashi (Ed.), ISBN: 978-953-307-980-6, InTech, Available from:
http://www.intechopen.com/books/application-of-thermodynamics-to-biological-and-materials-science/the-sintering-behaviour-of-fe-mn-c-powder-system-correlation-between-thermodynamics-and-sintering-pr

INTECH
open science | open minds